

Contact Line Laws For Spreading Fluid Droplets

G14PJA = MATH4041

Mathematics 3rd Year Project

Autumn 2021/22

School of Mathematical Sciences

University of Nottingham

Doug Lawes

Supervisor: Dr. John King

Assessment type: Investigation

I have read and understood the School and University guidelines on plagiarism. I confirm that this work is my own, apart from the acknowledged references.

Abstract

This investigation is about modelling the action point of the boundary between a fluid droplet and the surface said droplet is spreading over, known as the contact-line, when acted upon by gravitational and tensional forces. This will be done by investigating a known non-linear PDE that models the spreading of a fluid droplet after contact by forming a numerical solution using the Method of Lines, and will involve testing the effects of varying the boundary conditions used, the ratio of surface tension to gravity and the initial state. The efficiency of this numerical solution will be tested using comparisons to the real world expected and observable effects of changing these variables, and hence the result will support a specific weighting of forces and boundary conditions to match the model to realistic expectations.

Contents

1	Introduction	2
2	The Problem and the In-Built Numerical Solution	3
2.1	Background	4
3	Method of Lines Recreation	6
3.1	Gravity Only	7
3.2	Surface Tension Only	9
3.3	Both Forces	11
4	Testing Dependence On Variables	15
4.1	Contact-Line Plots (Cross-Sections in Height)	15
4.2	Cross-Sections in Time at the Boundary	18
4.3	Cross-Sections in Time for Changing Tension	22
4.4	Cross-Sections in Space	23
5	Changing Initial Conditions	28
5.1	Initial Width and Alternate Functions	29
5.2	Setting Initial State Before Contact	31
5.3	Unrealistic Initial States	34
6	Conclusions	39
A	Raw data	42
A.1	42
A.2	42

1 Introduction

The ability to model how a fluid droplet acts while spreading on a non-porous surface is useful in numerous applications, such as in water-flow management, battery production and in developing household appliances. One such known model to portray this spreading action comes from a more advanced variation of the heat equation PDE, which models temperature gradients in a closed room, by inserting an h^m term inside one of the partial x derivatives. The aim of this review is to analyse one such specific case of this where $m = 3$, and to find whether this model is sufficient to portray a droplet spreading in a real world scenario.

By the end, it will become clear that the model has its shortcomings, such as being limited to scenarios involving no resistive forces on the surface, meaning it can't portray different surfaces and fluids of varying viscosity, while also only accurately modelling droplets that have already made contact with the surface, so the physics of droplets in the air are also beyond its scope. Despite this, the model accurately portrays the result of taking the limit as the outer spatial values tend to their true value. Additionally, the effects of varying the spreading forces is also consistent with the real world, as scenarios driven by different forces end up with the same overall shape for a sufficiently large driving force, but also shows minute differences depending on which type of force is dominant. Then finally, it becomes clear that the main factor defining the rate of spread for a given fluid viscosity is defined by the volume of water dropped in the initial state.

These factors will be investigated in turn by observing different perspectives of the overarching surface plot of height, space and time while varying the proportion of force, initial conditions and boundary conditions.

2 The Problem and the In-Built Numerical Solution

The aforementioned PDE is portrayed as such

$$\frac{\partial h}{\partial t} = \frac{\partial(h^3 \frac{\partial h}{\partial x})}{\partial x}$$

$$h = e^{-x^2} + 10^{-3}, h(x = + - 10, t = 0) = 10^{-3}$$

The first matter at hand is to investigate the known equation to model a fluid droplet using the built-in Matlab parabolic PDE solver, pdepe [2], to have a known solver of the equation before attempting to design a more malleable one later on. This can be done by putting it in the form

$$c(x, t, u, \frac{\partial u}{\partial x}) \frac{\partial u}{\partial t} = x^{-m} \frac{\partial}{\partial x} (x^m f(x, t, u, \frac{\partial u}{\partial x}) + s(x, t, u, \frac{\partial u}{\partial x}))$$

with the boundary conditions

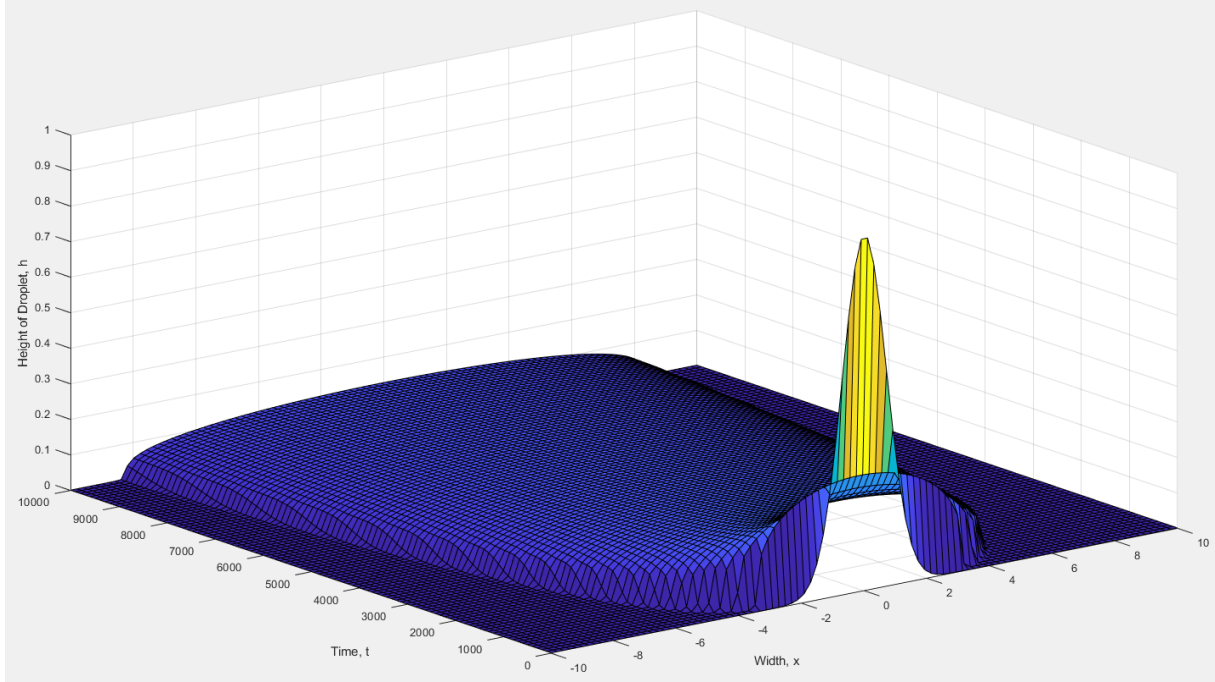
$$p(x, t, u) + q(x, t) f(x, t, u, \frac{\partial u}{\partial x}) = 0$$

Which in this case means

$$1 * \frac{\partial h}{\partial t} = x^0 * \frac{\partial}{\partial x} (h^3 \frac{\partial h}{\partial x}) + 0,$$

$$h - 10^{-3} = 0 = p(-10, t, h) = p(10, t, h)$$

And finally, the function produced the plot



Showing how the one-dimensional spatial droplet evolves in height over time (for a specific time scale).

2.1 Background

The PDE above is a specific case of the general fluid equation given by

$$\frac{\partial h}{\partial t} = \frac{\partial(h^m \frac{\partial h}{\partial x})}{\partial x}$$

Where the other specific case of $m = 0$ is known as the *Heat Equation*, and has a known solution given by

$$\text{Temperature} = e^{-\pi^2 t} \sin(\pi x)$$

Which is useful to check the accuracy of numerical methods before applying them to the more complicated $m = 3$ case.

Regarding the $m = 3$ case, one can alternatively use an exact solution method known as Similarity Solutions, which uses rescaling variables to rewrite the PDE as a singular combined function of the invariant terms under the aforementioned rescalings, and hence output a solvable ODE. This is mostly beyond the scope of this investigation, as it deals with exact

solutions, but will become useful when analysing the rate of spreading on the contact-line (section 4.1) and on vertical cross-sections (section 4.4).

Here, we use the rescalings $(x^*, t^*, h^*) = (\alpha^p x, \alpha t, \alpha^q h)$ to rewrite the PDE as a time-homogeneous ODE by finding the similarity reduction function

$$h = t^q f\left(\frac{x}{t^{\frac{3q+1}{2}}}\right)$$

With intermediary steps omitted, which, when combined with conserving mass using

$$\int_{-\infty}^{\infty} h dx = M$$

Gives specific values for the scaling powers of $p = \frac{1}{5}$, $q = -\frac{1}{5}$ and $h = \frac{3t^q}{10}(a^2 - \frac{x^2}{t^{\frac{3q+1}{2}}}^2)^{\frac{1}{3}} = \frac{3t^{-\frac{1}{5}}}{10}(a^2 - x^2 t^{-\frac{2}{5}})^{\frac{1}{3}}$ for $\eta = \frac{x}{t^{\frac{1}{5}}} < a$, else $h = 0$, where the latter comes from setting $h = 10^{-3} \approx 0$ and $t > 0$ (as h doesn't take a value there, and one can also vary the method of placing the droplet, which is portrayed by the initial condition equation given in the prior set-up, as will be investigated in section 5), which only works for the bracket being negligibly close to 0, so $a = \pm \frac{x}{t^{\frac{1}{5}}} = \eta$ at the boundary, and thus x is proportional to $t^{\frac{1}{5}}$ there, so when plotting height against one-dimensional space, the expansion of the boundary in space is much slower relative to the time elapsed, which is as shown in the prior plot.

3 Method of Lines Recreation

Now we must recreate the in-built solver from scratch, so as to investigate how the system evolves in a more general case. This is done using the Method of Lines, which discretises the system in terms of x , while leaving t continuous. This means the equation can be solved as a system of ODE's as opposed to the parabolic PDE above; metaphorically splitting our problematic loaf of bread (PDE) into uniform slices (ODEs).

On the known heat equation, formulated as

$$\frac{\partial h}{\partial t} = \frac{\partial^2 h}{\partial x^2} - a \times \frac{\partial^4 h}{\partial x^4}$$

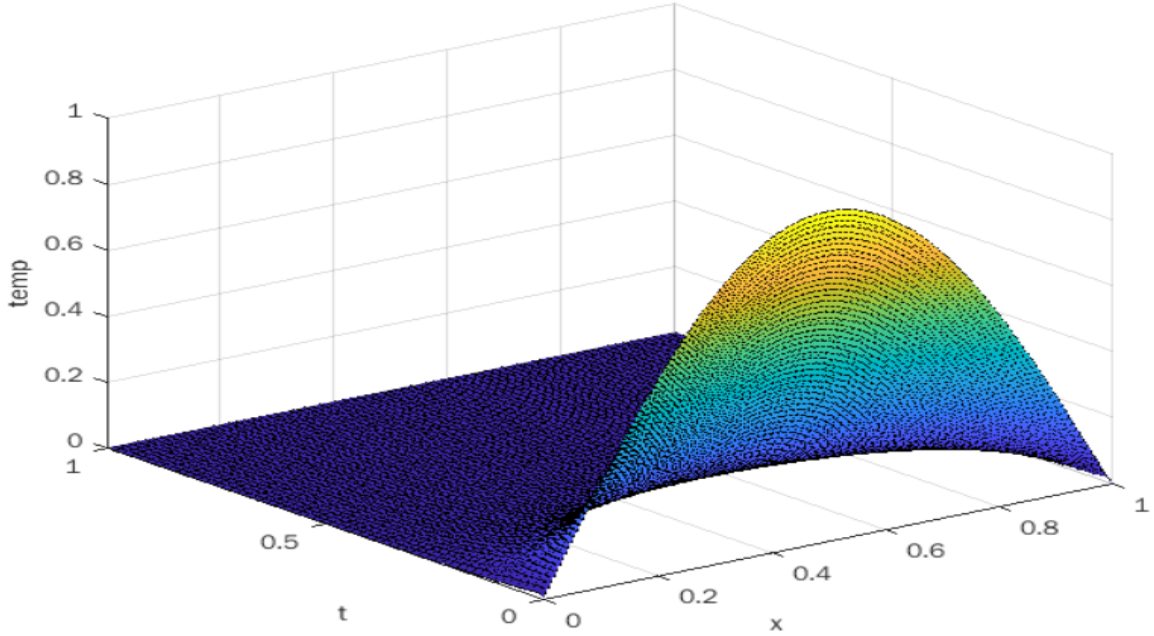
This method uses the central difference theorem to discretise the right-hand side, and since both of the derivatives are of even order, one can use the known equations

$$\frac{\partial^2 h}{\partial x^2} = \frac{h_{i+1} - 2h_i + h_{i-1}}{\Delta x^2}$$

and

$$\frac{\partial^4 h}{\partial x^4} = \frac{h_{i+2} - 4h_{i+1} + 6h_i - 4h_{i-1} + h_{i-2}}{\Delta x^4}$$

To discretise the equation in terms of individual h_i 's. Which overall approximates the heat equation very closely for a relatively low resolution model, where in this document we will mostly use two-hundred steps in the interest of showing both the slight discrepancies caused by a low resolution, but also being high enough resolution to mostly match the algebraic solutions. This is overtly shown by plotting the approximate heat equation:



Which exactly matches the shape expected to be formed by the algebraic solution, with only minor displacements¹ from it for values close to the initial state.

3.1 Gravity Only

Now repeating this method on the droplet equation is more difficult, as there are embedded derivatives, so we reformulate the problem as

$$\frac{\partial h}{\partial t} + \frac{\partial J}{\partial x} = 0, \quad J = -h^3 \frac{\partial P}{\partial x},$$

and then use the central difference theorem on both equations using a half-step in time, which will cancel when substituted

$$\frac{\partial h_i}{\partial t} = \frac{J_{i-\frac{1}{2}} - J_{i+\frac{1}{2}}}{\Delta x}, \quad J_i = -\left(\frac{h_{i-\frac{1}{2}} + h_{i+\frac{1}{2}}}{2}\right)^3 \frac{P_{i+\frac{1}{2}} - P_{i-\frac{1}{2}}}{\Delta x}$$

Which gives the overall equation for the vector of h_i values as

$$\frac{\partial h_i}{\partial t} = \frac{(h_i + h_{i+1})^3(P_{i+1} - P_i) - (h_{i-1} + h_i)^3(P_i - P_{i-1})}{8\Delta x^2}$$

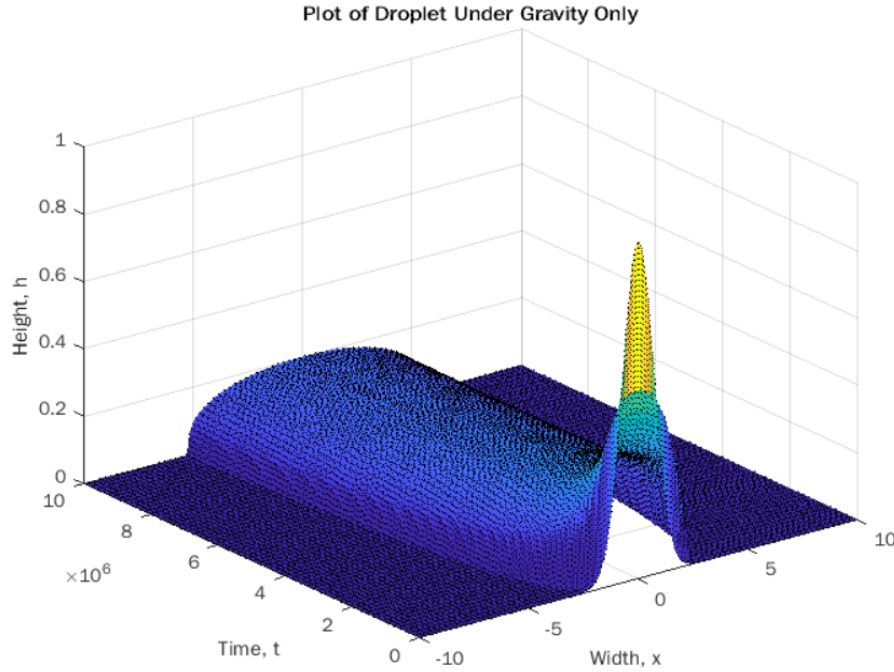
¹See section A.1 for error array

For P representing pressure.

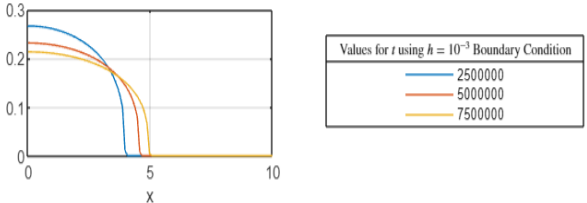
Now the simplest solution is by negating all forces except the dominant gravitational force, which is done by subbing in the above J 's and assuming no surface tension, which means the pressure is equivalent to the thickness of the droplet above the surface, h , hence

$$\frac{\partial h_i}{\partial t} = \frac{(h_i + h_{i+1})^3(h_{i+1} - h_i) - (h_{i-1} + h_i)^3(h_i - h_{i-1})}{8\Delta x^2}$$

With this setup, we need to set the Boundary Conditions as the x values at the extremities [1], and define a system of ODE's attributed to each individual h_i as above. We can then use the inbuilt *ode15s* stiff ODE solver [2] to solve each h_i by giving values of arbitrarily small heights at the edges of the spatial boundary for the function to iterate in-between. We require a *stiff* ODE solver since a regular solver, such as *ode45* wouldn't account for the previous or next values of h_i . This gives a similar result to before, but with slight differences due to the Method of Lines being inexact for non-negligible step length. The value of Δx is directly proportional to the number of steps used, hence one can approximate Δx to be the width of the system (20 here) \div the number of x points. Notably, the plot of this function is already a close approximation to the in-built function, given that the plot of height is:



with the plot of the pres-



sure term ($P = h$ above) for discrete time being

3.2 Surface Tension Only

The next step is to incorporate surface tension, which accounts for a slight amount of run off in the model, which would be present for a fluid droplet on any hydrophilic surface. This is done by substituting

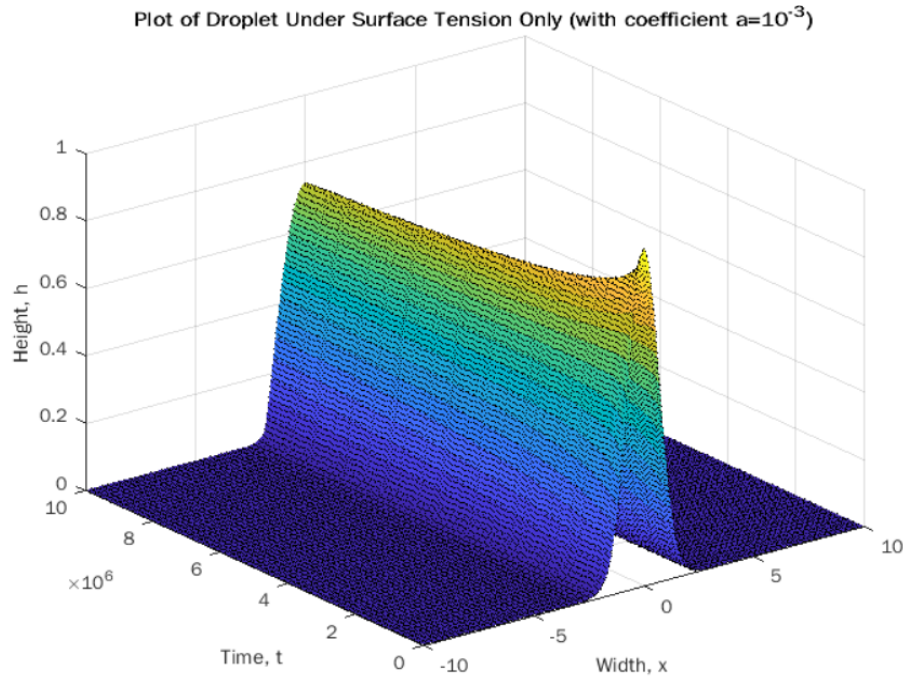
$$P_i = \frac{a}{\Delta x^2} (h_{i+1} - 2h_i + h_{i-1})$$

For pressure instead, for some small constant a , hence the impact of this change is small to the overall system, given that $a = 0$ yields just gravity if both forces are applied simultaneously. This model required using two extra boundary conditions at the spatial extremities, as substituting this for P in

$$\frac{\partial h_i}{\partial t} = \frac{(h_i + h_{i+1})^3(P_{i+1} - P_i) - (h_{i-1} + h_i)^3(P_i - P_{i-1})}{8\Delta x^2}$$

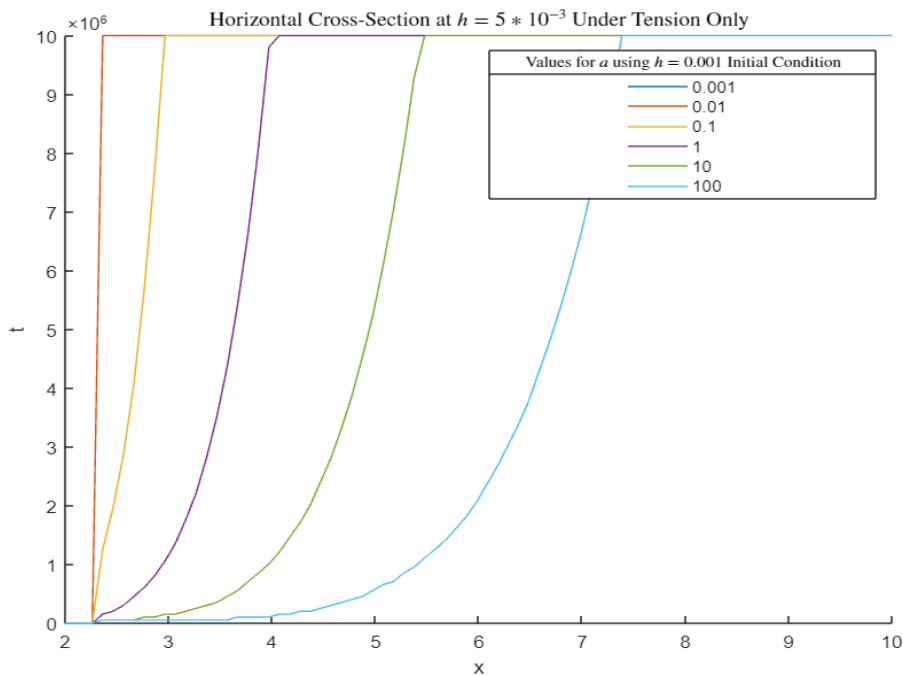
yields a reliance on the former and latter two values for h_i , so the first and last two x values in the range must all now be $= 10^{-3}$, which is a safe assumption as they are negligibly far away from this for the prior case, but the choice of order will be investigated further in section 4.2 once the model is complete.

Plotting this requires analysis of the aforementioned time-scale, since the h terms in P are on a time-scale of order $\text{Length}^2 \div h_{max}^3$, so $O(10^2)$, while the latter terms are on a time-scale of $\text{Length}^4 \div (a \times h_{max}^3)$, so is $O(10^7)$ for a choice of $a = 10^{-3}$. Therefore the surface plot on this time-scale for a specific small value of the coefficient looks like:



And the plot for many

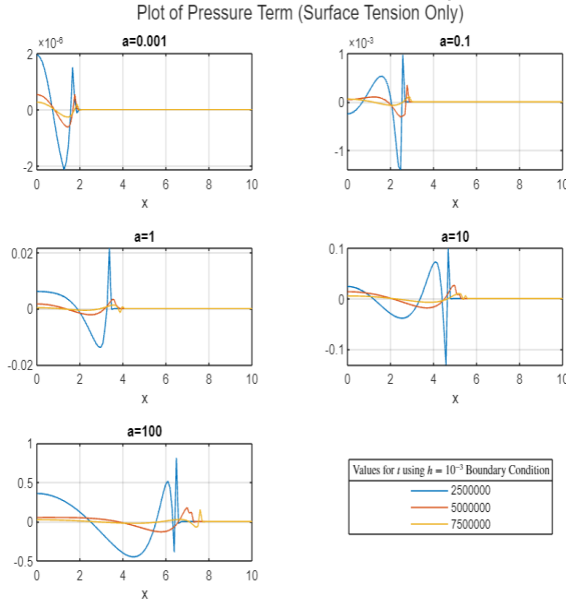
different coefficients of a is best portrayed by a contact-line plot (a horizontal cross-section), showing the evolution of the boundary between the droplet and surface, as will be explained in section 4.1.



This shows that when negating the gravitational term, the contact line begins to look like the boundary for the gravity inclusive cases as a increases, and undergoes very little spreading over time for small a , as the parameter is intended to be. This works in context, as without much surface tension or gravity acting on the substrate, it has no force driving it to spread, and

hence will remain stationary; whereas if surface tension is dramatically increased, the force will cause a surface run-off, pulling the droplet away from a stationary position, which, from this perspective, has the same effect as introducing a gravitational force.

However, the pressure plot for large a doesn't resemble that of the gravity only case at all, and instead shows how most of the pressure in this case is acting on the contact line.



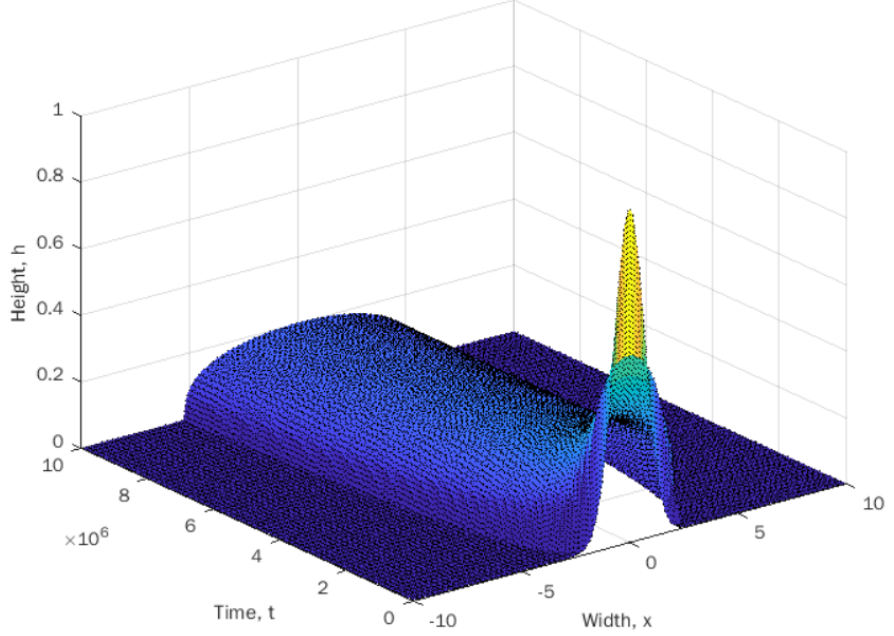
The most notable difference is that the pressure varies between positive and negative values, which is caused by the central difference theorem, in that the sum of the heights at the two adjacent positions are less than that at the current position, so the overall pressure is negative. This only happens at the boundary because of the large drop off of the model at the contact-line relative to the gradient up to that point. Therefore this model doesn't exactly show the base of the surface, and hence the line of contact should be at a slight displacement from the line $h = 0$ (e.g. $h = 5 \times 10^{-3}$ as in the prior plot).

3.3 Both Forces

Now combining these forces gives the final form for the droplet model

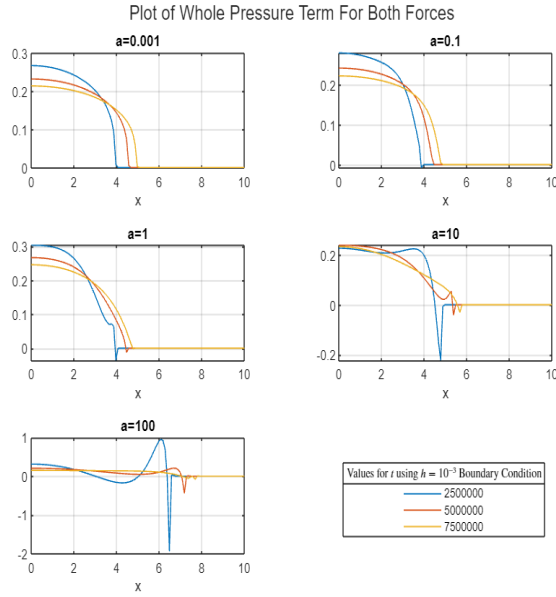
$$\frac{\partial h_i}{\partial t} = \frac{(h_i + h_{i+1})^3(h_{i+1} - \frac{a}{\Delta x^2}(h_{i+2} - 2h_{i+1} + h_i) - h_i + \frac{a}{\Delta x^2}(h_{i+1} - 2h_i + h_{i-1}))}{8\Delta x^2} - \frac{(h_{i-1} + h_i)^3(h_i - \frac{a}{\Delta x^2}(h_{i+1} - 2h_i + h_{i-1}) - h_{i-1} + \frac{a}{\Delta x^2}(h_i - 2h_{i-1} + h_{i-2}))}{8\Delta x^2}$$

Plot of Droplet Under Gravity and Surface Tension (with coefficient $a=10^{-3}$)



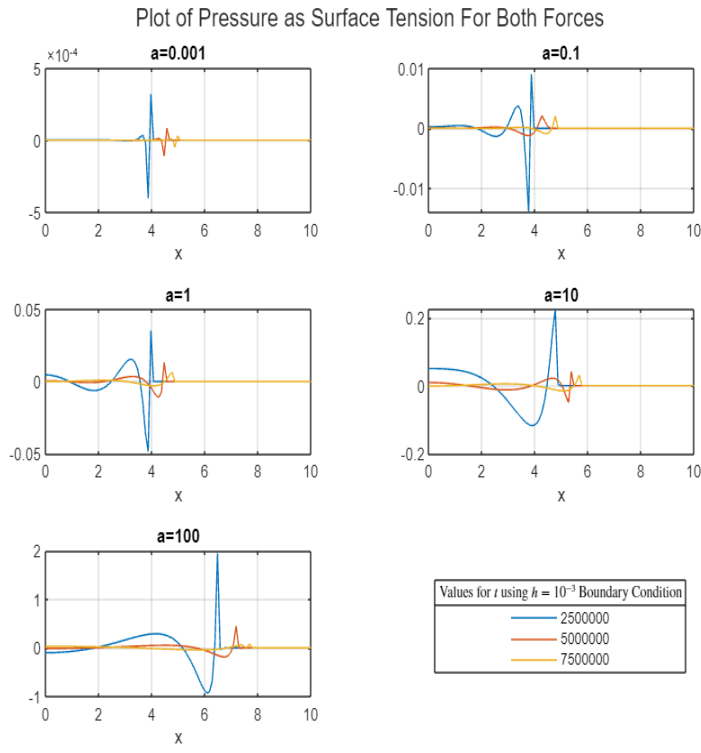
Which looks like:

Where the corresponding pressure term $P_i = h_i - \frac{a}{\Delta x^2}(h_{i+1} - 2h_i + h_{i-1})$ looks like



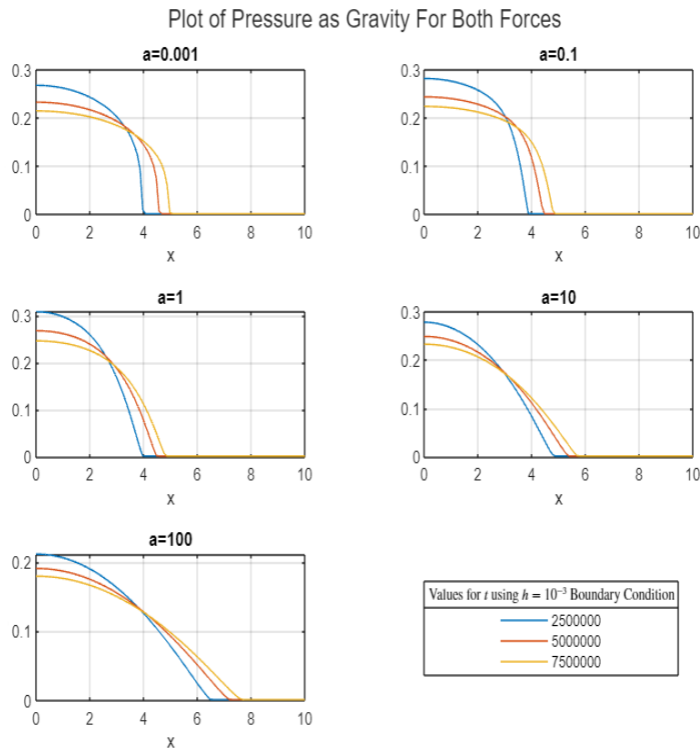
for varying a and time values, which shows how the pressure at small $|x|$ remains mostly constant for increasing tensional forces, but the pressure on the contact-line gets geometrically larger, and doesn't resemble the gravitational pressure plot beyond $a = O(1)$.

One can also investigate the effects of just the individual force components of the P term, calculated using the total force equation, which are



Where positive values are where P

is lower as a result, and vice versa for negative values, and the gravity case is as before



This shows how close to $x = 0$, the effects of surface tension are minimal, whereas elsewhere in the space the effects can drastically change around a pivot point that depends on the value of a . For small a this is around $x = 4$, but as a grows, the frequency of this damped-sinusoidal oscillation spreads out, slowly moving the pivot closer to the edges of the domain. This pivot

point acts as the difference between points closer to the drop site that decrease in substrate height at a specific time as a result of the increasing amount of surface tension, and points closer to the edge that increase in height under the same conditions, overall causing a decrease in the contact angle at the edges.

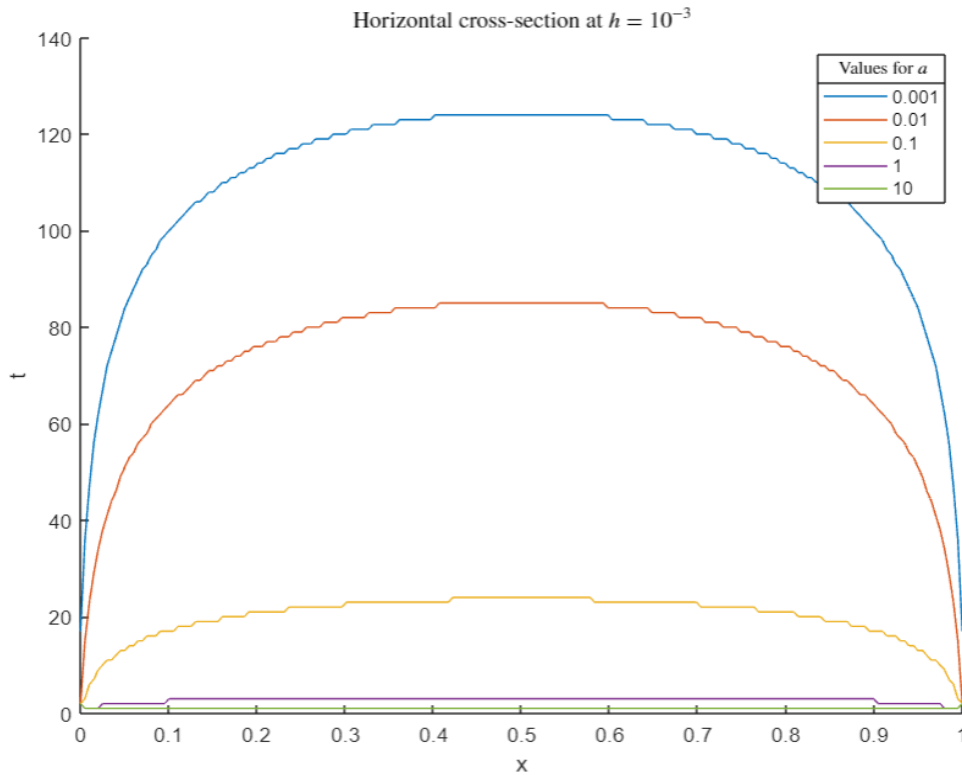
Notably also, the effect of increasing a by a magnitude of 10 on the tension only pressure plot increases the amplitude by a factor of 5 each time, which isn't the case for the gravity only pressure plot. Therefore given that a starts arbitrarily small, there is an a such that the tensional force is equivalent to the gravitational force, and will surpass it. This will be a frequent occurrence in the remainder of the investigation.

4 Testing Dependence On Variables

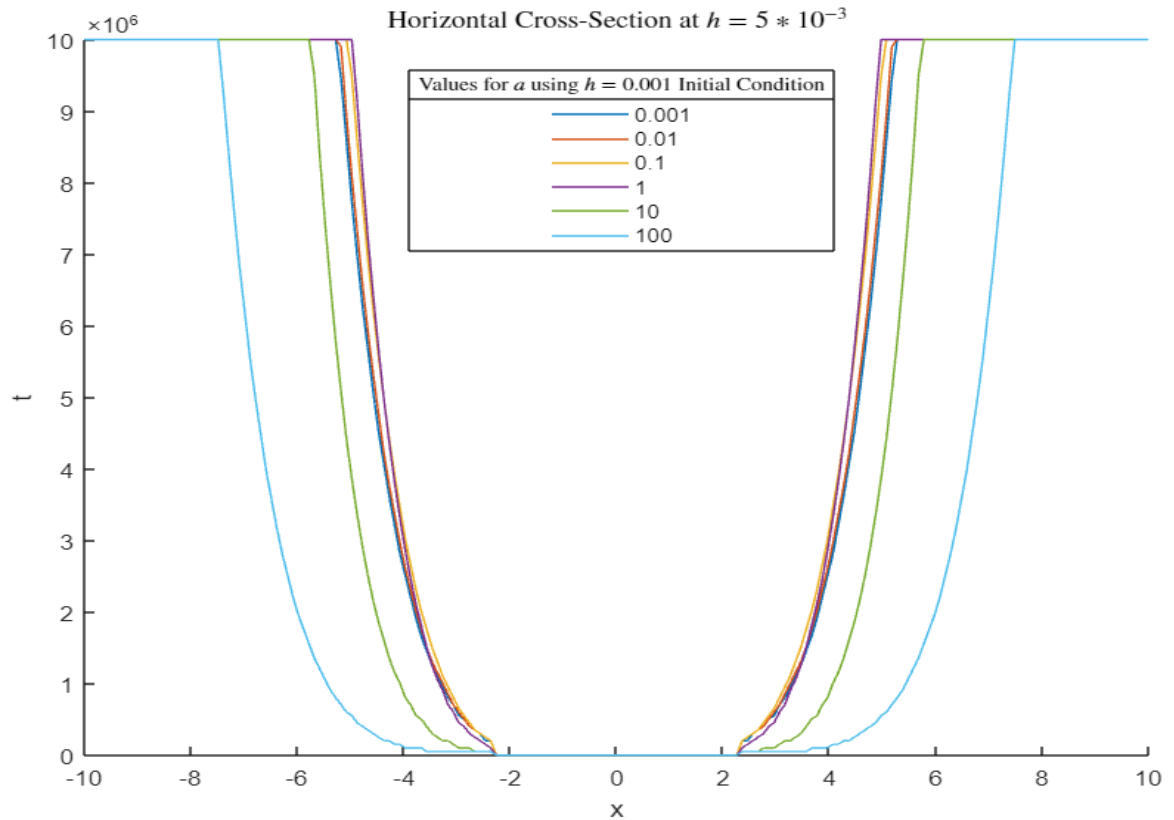
Now that we have a model with a scaling variable a and arbitrary displacement 10^{-3} , it is prudent to see how varying a for different values of boundary conditions affects the model.

4.1 Contact-Line Plots (Cross-Sections in Height)

Another way of visualising the prior surface plots is by using contact-lines, which are the lines of intersection between the surface plot of space, time and height, against a plane at a fixed height close to zero, e.g. some multiple of the boundary condition used as in section 3.2. This gives a plot of space against time, which shows the time at which the height of the droplet goes below the threshold value at any point in space. As an example, the contact lines for the linear Heat equation used prior are:

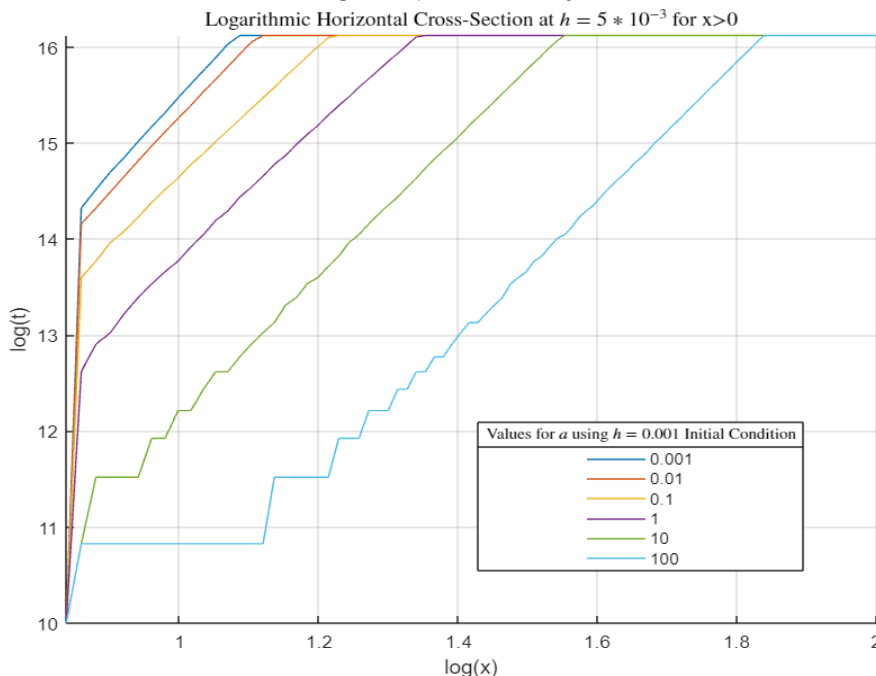


Therefore by setting the threshold value to be $h = 5 * 10^{-3}$, the contact-lines for the a 's used thus far are:



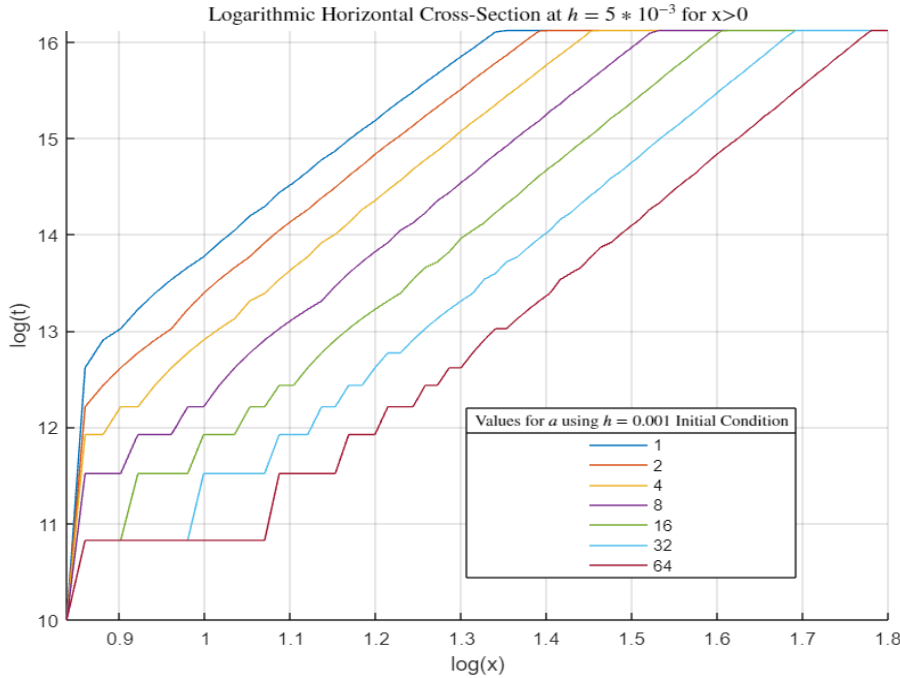
which shows how the system is consistent for α up to a point; after which changes will have a dramatic effect on the spreading rate.

This can be investigated further looking at the logarithmic plot, plotted on half of the spatial dimension, where the straight top line is only due to the maximum time scale used.

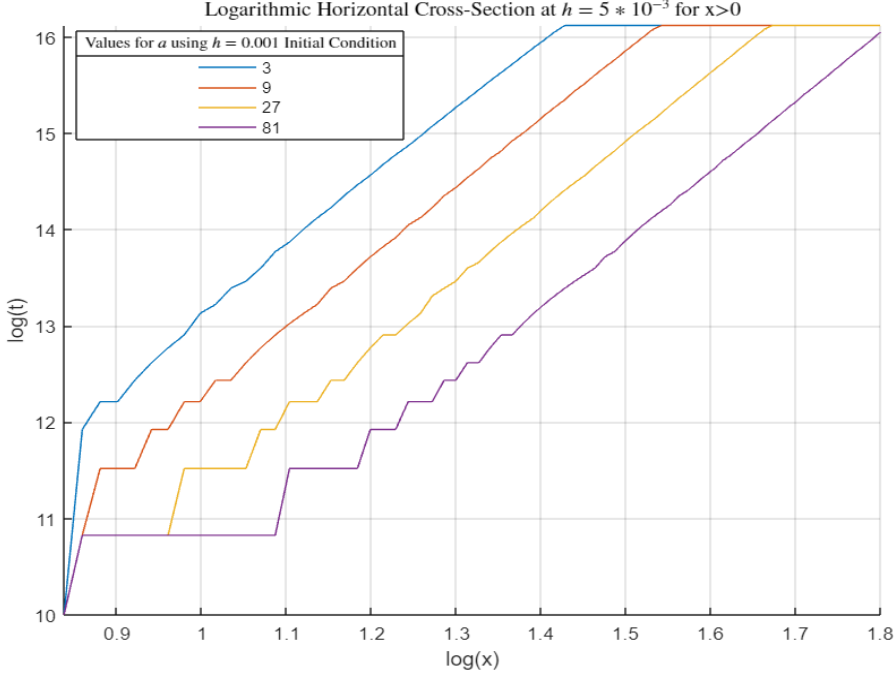


This shows how the contact line, represented by its corresponding x value, is translated in

time at an increasing rate proportional to a . This proportionality becomes more apparent when values of a in a geometric series are plotted instead, giving



Which shows an approximately constant linear decrease in time for each power of two increase in a . This is also true for k^{th} geometric series as well, as is evident in the powers of three:



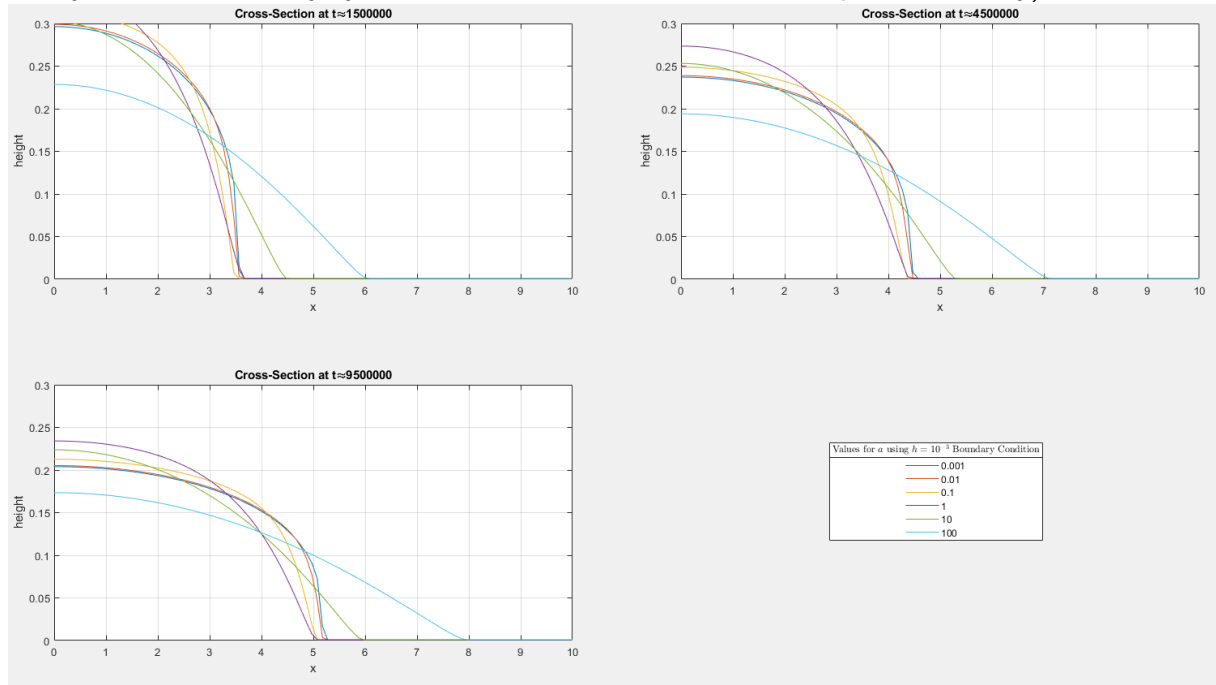
Therefore it's notable that increasing a has diminishing returns, in that it requires a to become quite a bit larger to maintain the same rate of change in spreading rate.

Also notably, the gradient of the "loglog" line is constant, and can be found by setting $h = 0$ in $h = \frac{3t^{-\frac{1}{5}}}{10}(a^2 - x^2 t^{-\frac{2}{5}})^{\frac{1}{3}}$, simplifying down to a constant power ($\approx \frac{1}{5}$ here) which is evident for

all a beyond a threshold t value. Therefore linearity is consistent for all relevant proportions of surface tension, but only for points beyond a certain spatial distance away from the drop-site, as is evident in the $a = 10$ and $a = 100$ lines having horizontal components near the origin. This suggests that the initial rate of spreading isn't contained in the logarithmically linear shape of the contact-line, but instead based on the interaction between the initial state and the dominant force, as increasing the proportion of surface tension to gravity will eventually lead to surface tension overpowering the force of gravity, and will cause differing effects to the exact solution investigated in section 2.1 (as will be investigated in section 4.4).

4.2 Cross-Sections in Time at the Boundary

Next, for 10^{-3} which has been used so far on the boundary, the following cross-sections of the model show how the contact angles and lines change for different points in time at the boundary (note only small t has been used since the model is consistent beyond a limit, and the system is necessarily symmetric at all values, so these show positive x only):

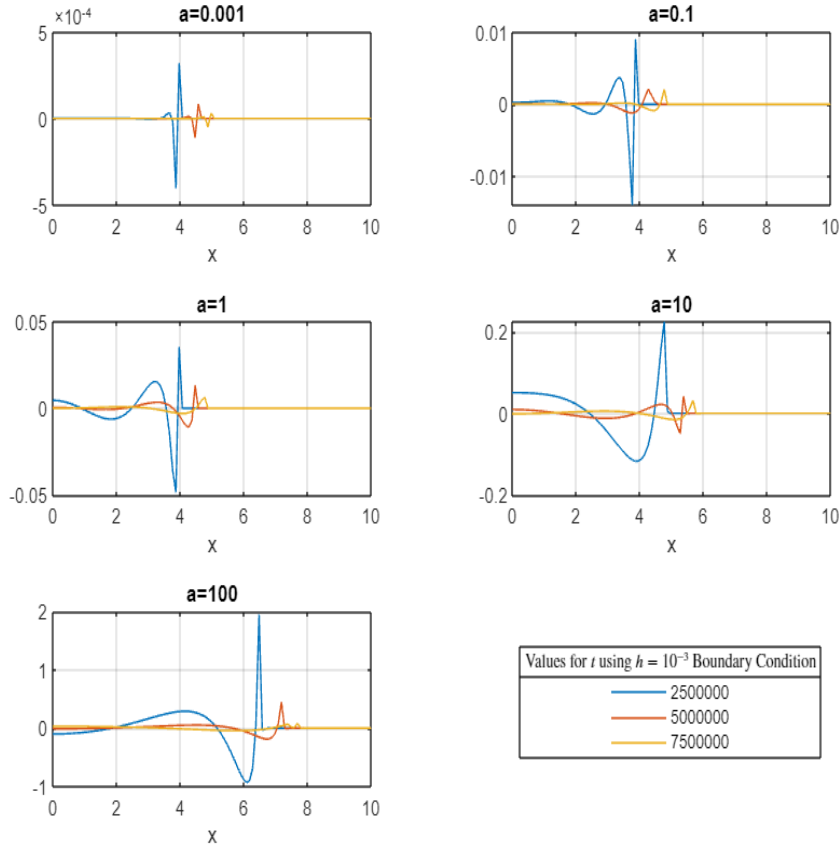


These show how increasing a leads to a shallower decline on the edge of the contact line, but with a lower central value (will be investigated in section 4.4), which initially seems more realistic in context.

The most important observation however, is in relation to the aforementioned pivot points in

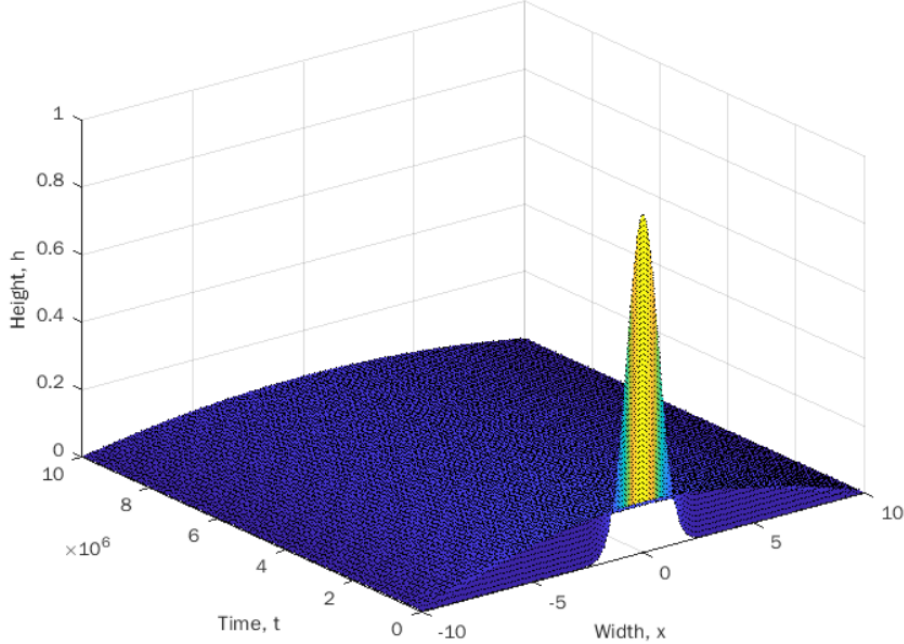
section 3.3, where the plot of pressure for the tension only case:

Plot of Pressure as Surface Tension For Both Forces

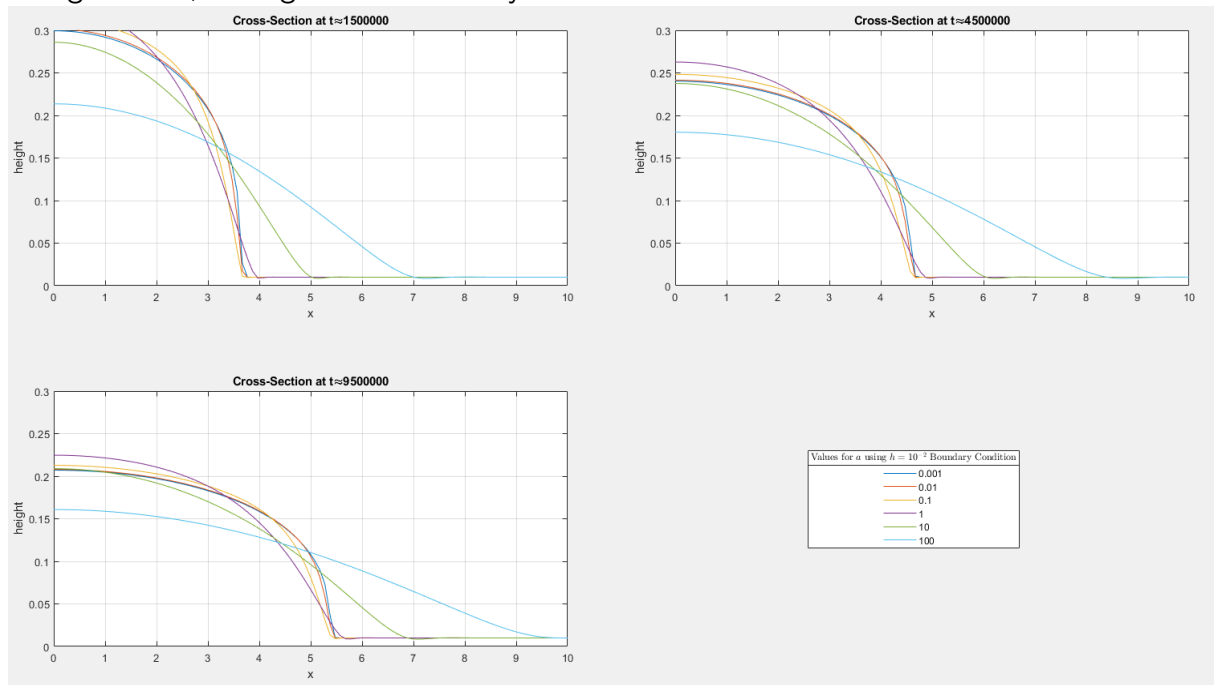


Shows that the roots of the cross-sectional lines in discrete time line up closely to the “pivot” points where pressure forces oscillate the most (when accounting for slightly different times used, where values in plots were chosen to best represent the changing shapes). This means the tensional force has a disproportionate effect on the shape of the boundary between empty space and the droplet, and acts to supplement the gravitational force, which has a pressure proportional to the height of the droplet at all times. Therefore, higher tensional forces would cause large changes on the shape and spreading rate at the boundary, and so would have an effect on the spreading rate at the drop-site, as the overall volume of water, calculated by the area underneath the cross-sectional plot of height against space, must remain constant at all times for a non-porous surface, and for all ratios of surface tension to gravity. This supports setting the tensional force to be relatively small ($a = 10^{-3}$) since as tension increases, the rate of dispersion at the drop-site increases, so for tension beyond a threshold, the rate of dispersion becomes unrealistically fast, even for a system negating frictional resistive forces, and will be in breach of the first law of thermodynamics governing conservation of energy.

Plot of Droplet Under Gravity and Surface Tension (with large coefficient a)



Alongside this, testing for the boundary condition 10^{-2} as such



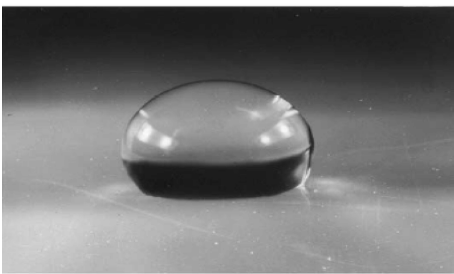
Shows a similar shape to before, but with a small decrease in incline for any given t , which suggests that increasing the boundary values has an inversely proportional effect on the rate of fluid dispersion. For this model, we use 10^{-3} as an arbitrarily small value, hence ideally this would be as close to zero as possible. Therefore, these findings suggest that the rate of fluid dispersion either tends towards zero, which is unrealistic for non-hydrophobic surfaces, or that there exists some minimal value for the rate to be found. These results are encouraging, as

there is no case in the real world where the rate of dissipation is infinite, which would require a surface with no frictional forces, whereas there are cases where the droplet would spread slower, tending towards even stable states.

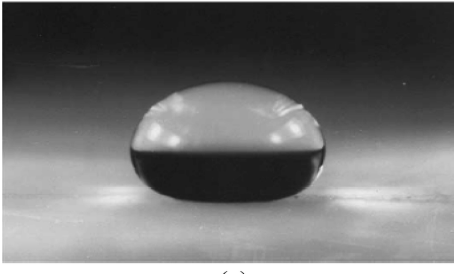
This behaviour is evident in products such as Aerogel [3], which has the properties of low thermal conductivity, a very high surface area per unit volume, and most notably in this case, can be made to be almost completely hydrophobic. However, the contact angle of the system modelled above doesn't go beyond 90° , but the contact angles, measured from the horizontal centre of mass, of different combinations of Aerogel and a hydrophobic component can go far beyond this, as shown here [4]:



(a)



(b)



(c)

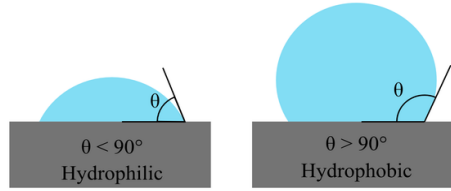
showing a) The MTMS component reaching a contact angle of 95° , b) TMMS at 125° and c) HMDS at 135° , hence showing how our model is insufficient for some surfaces².

This adds another restriction to the system presented, as this model only accounts for surfaces with greater wettability, defined as being "the measurement of liquids' ability of interaction with other fluids and/or solid surface" [8], but with negligible frictional forces, while these

²See section A.2 for the full dataset

Aerogel components show other, less wettable cases that cannot be modelled using this representation.

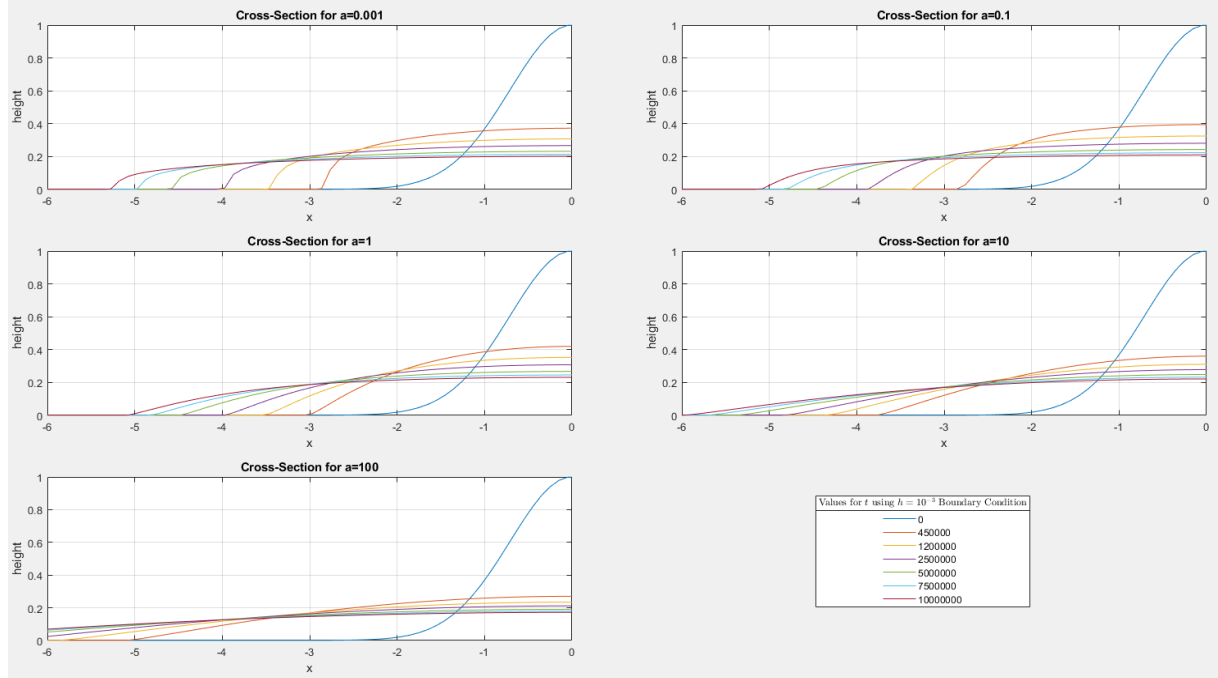
These situations can be sorted into hydrophobic and hydrophilic by setting the threshold value at 90° , e.g. [9]:



And therefore put succinctly, our system uniquely models hydrophilic surfaces.

4.3 Cross-Sections in Time for Changing Tension

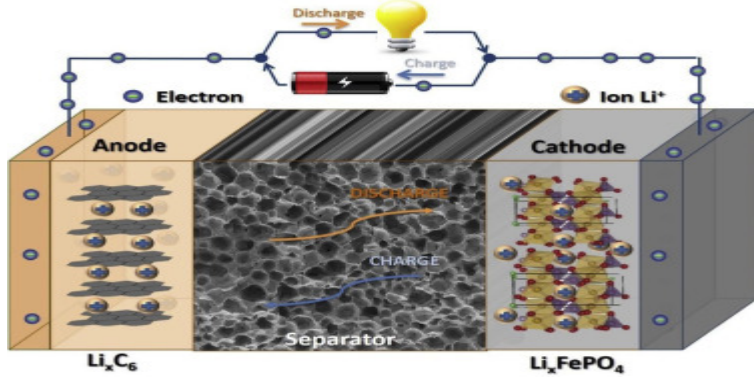
Thus far, visualisations for the entire solution curve at discrete time have been at the boundary exclusively, however, one can also plot cross-sections in discrete time against each other for a given value of a as below:



Which shows how the spreading action over time increases as a increases, and additionally again shows how the action at the contact line is less jagged for higher a . This is encouraging, as the effects of increased surface tension on a constant gravitational force would make the droplet sit much closer to the surface and would make it spread faster than it would otherwise;

which matches the above figure.

This model has thus far run on the assumption that the surface is “ideal”, which defines it as being “rigid, perfectly smooth, chemically homogeneous, and with zero contact angle hysteresis” [7]. However, in real world situations, such as in the production of sodium batteries [10], accurately measuring the contact angle at discrete times is important to measure the wettability of a ‘separator’ between the anode and cathode;

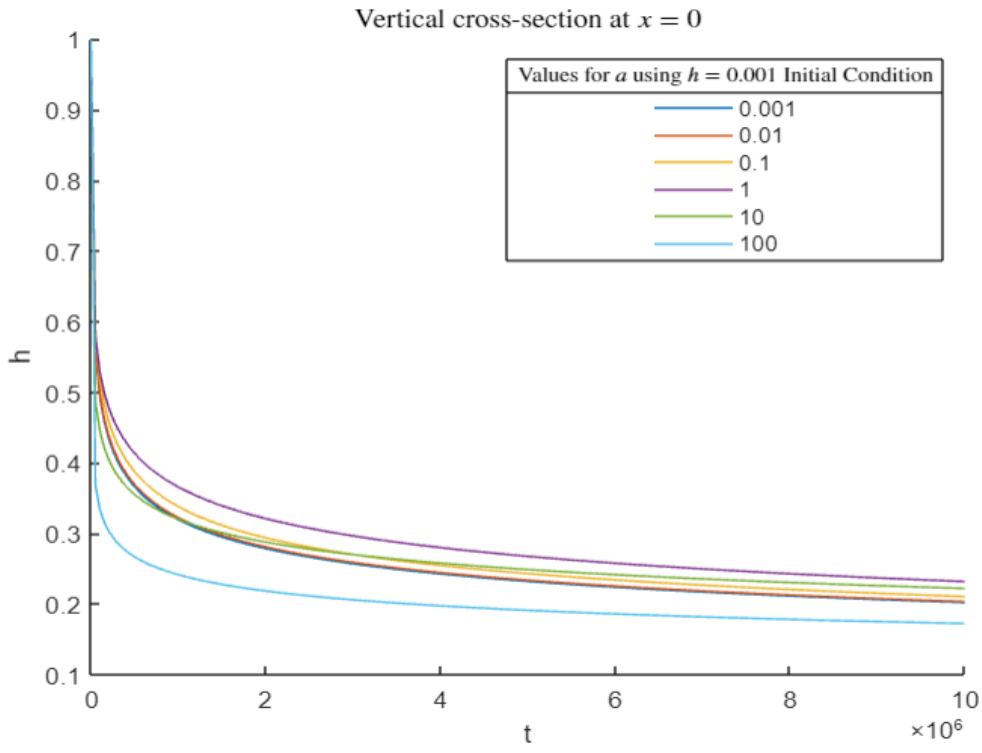


[11] where water (electrolyte) droplets

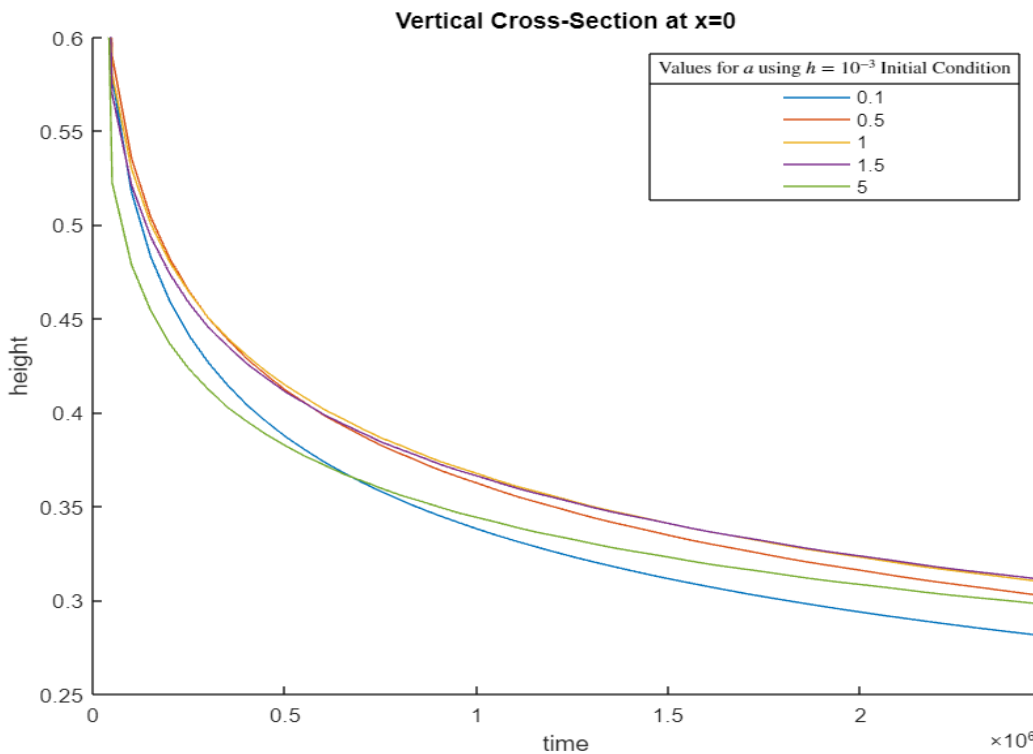
simulate the porosity of the separator material, and good quality separators “should be able to absorb a significant amount of electrolyte and also reserve the absorbed electrolyte when the cell is under operation” [10].

4.4 Cross-Sections in Space

Now that the change at the boundary has been examined, the rate of change along the principle line, $x = 0$, should be examined to see whether increasing a has a linear effect on the rate of spreading of the droplet (portrayed by the slope of decreasing height at the drop-site), which, for the $h = 10^{-3}$ boundary condition, is:

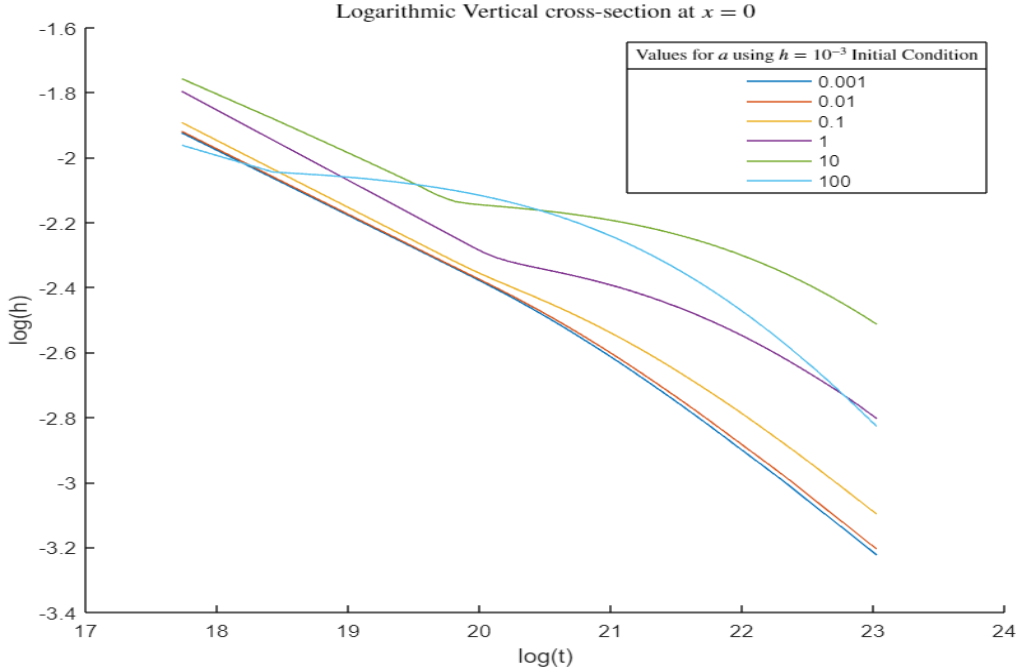


Which shows an interesting relation between height and a , given that $a = 1$ is the slowest to decrease, with values below that growing linearly up to that value, but then for $a > O(10)$ the height of the droplet starts decreasing faster than before. Therefore, there is theoretically an optimum value for a , the amount of surface tension, that causes the rate of decline in the centre to be minimum. So plotting at a higher resolution for a and smaller t gives:



Showing how at the slow time scale, the greater the value of a up to $a = 1$, the faster it initially decreases, but will level off faster. However, beyond $a = 1$, the only change is the initial drop-off (as in $a = 5$).

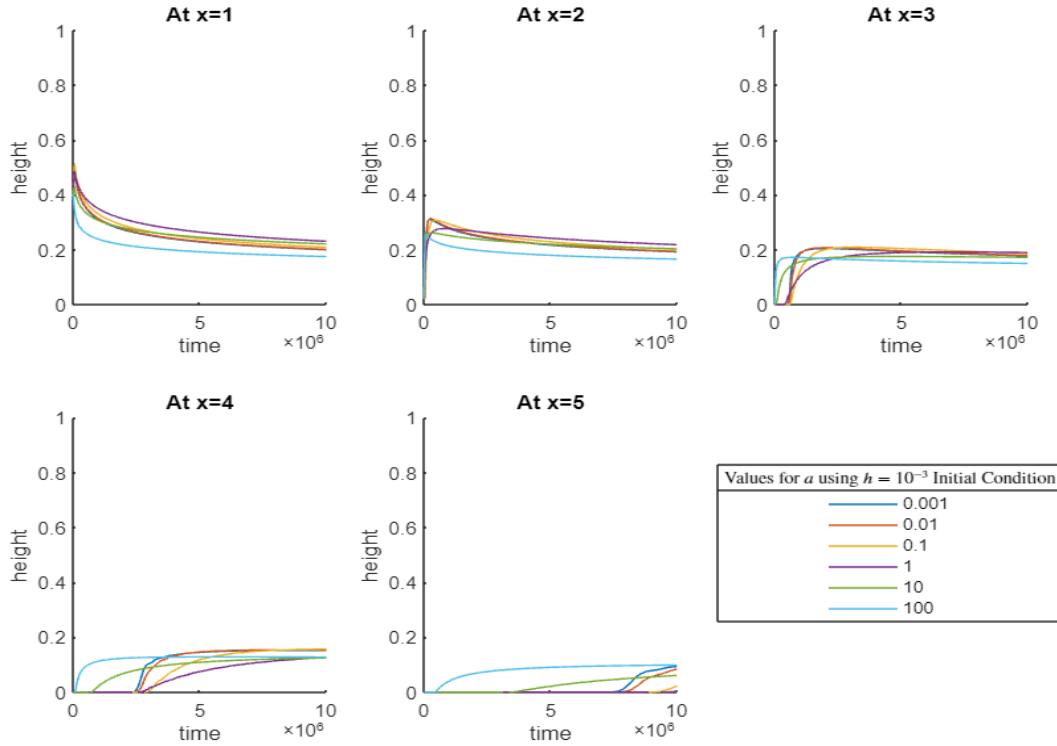
The difference between slow and fast time scales is more evident in logarithmic plots, where the non-linear start caused by the initial condition function (the act of producing the droplet) is converted into a linear function after sufficient time, as shown in the following:



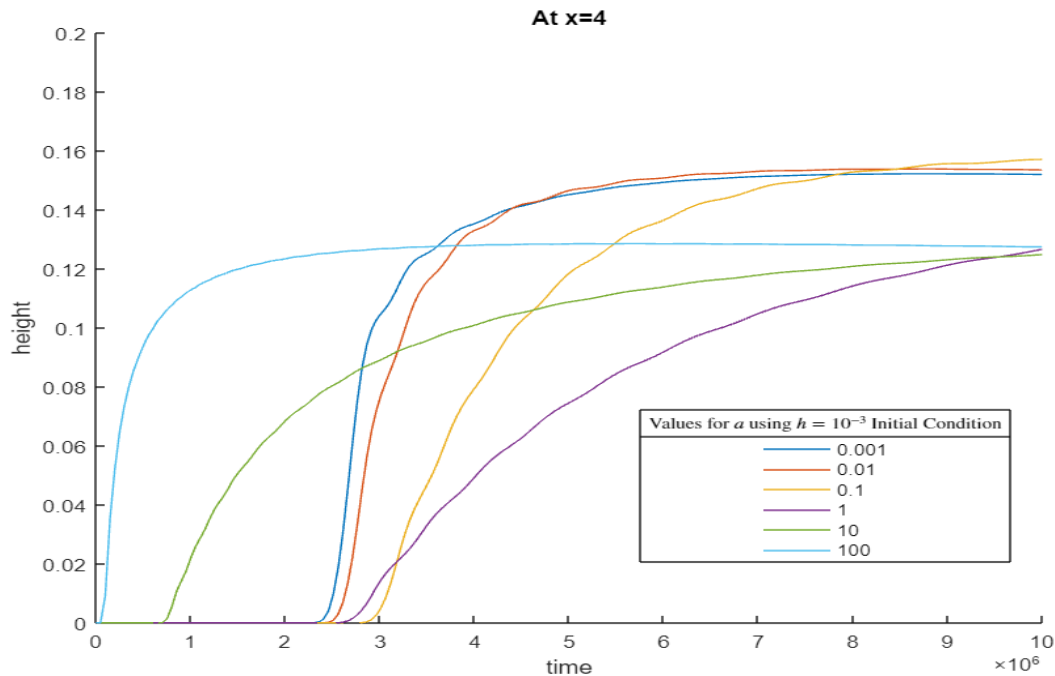
Where the gradient is determined by the invariants in the similarity solution investigated in section 2.1, $h = \frac{3t^{-\frac{1}{5}}}{10}(a^2 - x^2 t^{-\frac{2}{5}})^{\frac{1}{3}}$, where setting $x = 0$ gives the logarithmic gradient to be $-\frac{1}{5}$, which is approximately correct for small tension forces beyond a certain time threshold.

The fact that these lines for larger t are mostly parallel suggests that on the large time scale, all ratios of forces have the same spreading rate at the drop-site. However on the short time scale, it is obvious that the higher ratios of surface tension are completely non-linear, and instead resemble a quadratic shape. This echoes the idea in section 4.1 that on the short time scale, the spreading rate is mostly determined by the initial state and isn't based on the exact solution from 2.1.

Alternatively, one can examine the effects of changing the ratio of forces at different locations on the surface, such as in vertical cross-sections at the following x points

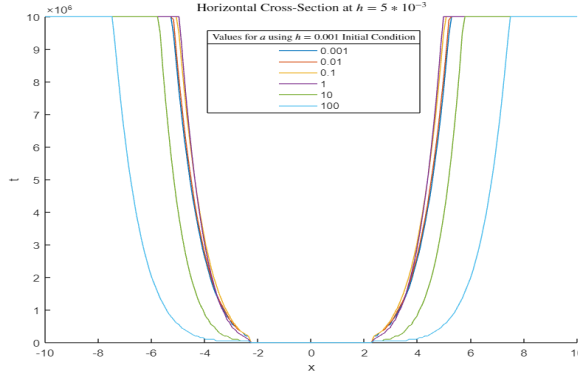


Where the effects around $a = O(1)$ are diminished at points in space that were originally defined by the $h = 10^{-3}$ portion of the initial condition, and instead the model shows how varying the forces gives different times that the droplet spreads to that position in space. Take, for example, the plot around $x = 4$:



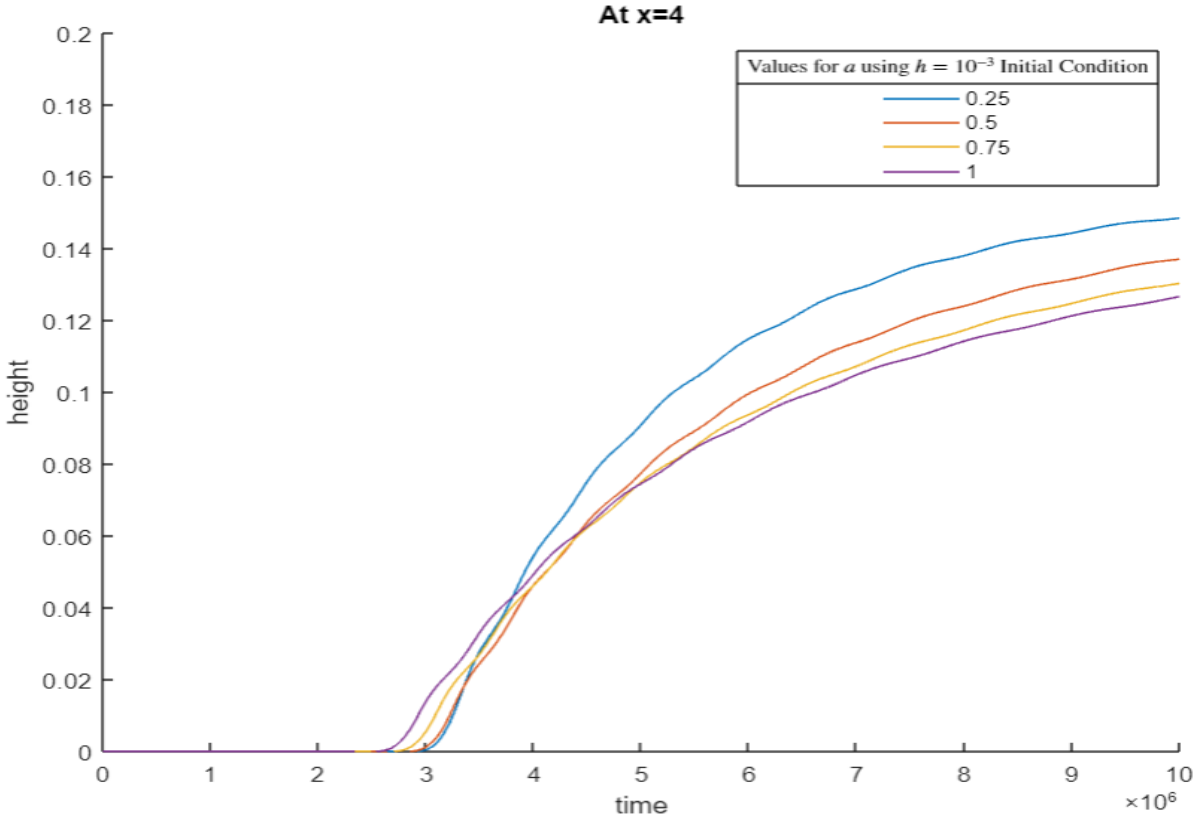
Which portrays another non-uniform effect of increasing surface tension in proportion to gravity. This is again caused by the surface tension overpowering the force of gravity, but now this

action is at a point on the contact line (an initially dry point on the surface), so increasing a doesn't just reduce the height intercept as in section 4.1 but now speeds up the time it takes the droplet to spread to this position. This action was evident in the prior contact line plot



Showing how the initial spread out for higher a is larger for all $|x| > 2$ (on the contact line).

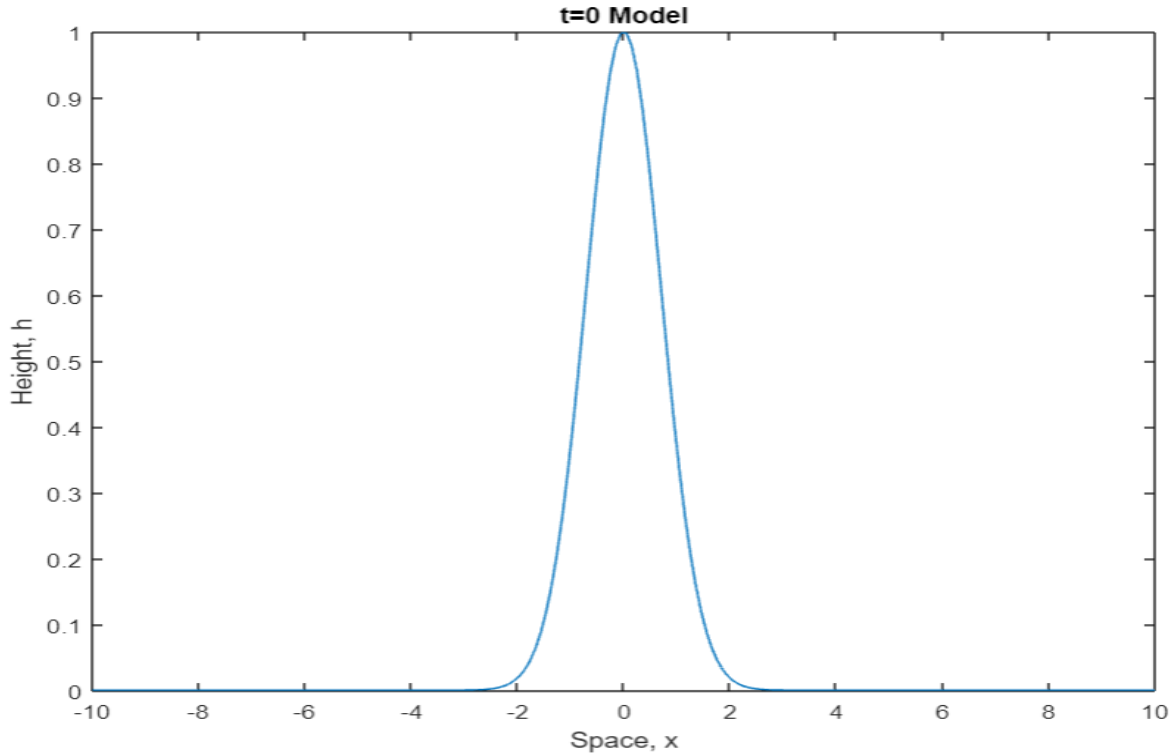
However, further investigation into $a = O(1)$ gives



Where the overlap is again evident between $a = 0.5$ and $a = 0.75$, further emphasising the change between a logarithmically linear solution for small a and a logarithmically "quadratic" solution as shown by the $a = O(100)$ line in the prior logarithmic vertical cross-section plot.

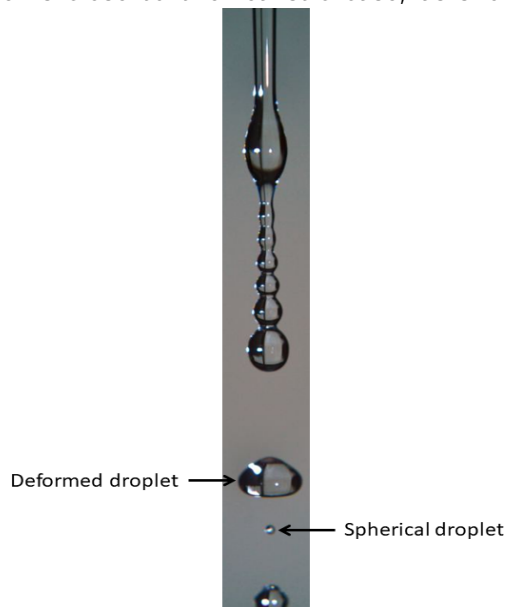
5 Changing Initial Conditions

Another variable in this model is the initial dropping method, thus far being exclusively modelled by $e^{-x^2} + 10^{-3}$, which visually is



Which is a specific case, given that the width, height and shape of the slope are all variable qualities of this model and can be changed to produce different effects on the spread.

However, this model is close to the realistic case, as shown by panoramic imagery taken by



Gaurav Singh [5]:

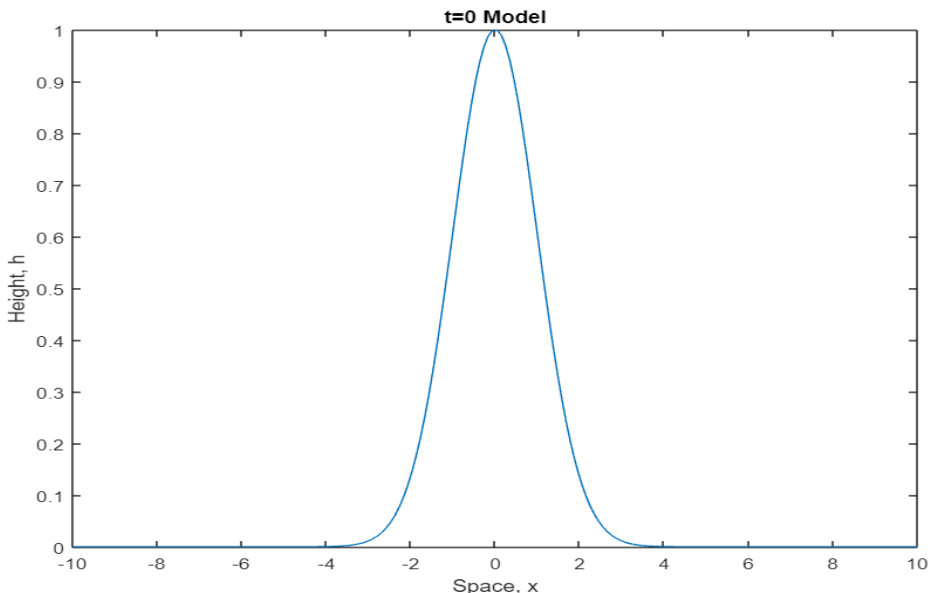
and annotated by Sumit Joshi [6]

as part of the latter's investigation into the splitting of water droplets exiting a tap. They

investigated the forces acting on a falling droplet and concluded that the “three major forces” acting on the droplet are i) gravity, ii) wind resistance (friction), and iii) surface tension (to the tap in that case). This is largely different to the flow happening in our model, as on the surface there is still gravity, but also a small surface tension force acting in favour of the spread, whereas this tensional force acts in opposition to the droplets motion. In addition to this, the frictional force isn’t accounted for in this model by assuming the surface the droplet is spreading on is sufficiently smooth, however this is a possible extension to the model if modelling a droplet on rough surfaces, such as roof tiles for construction work, is necessary. When comparing this to the above one-dimensional initial state, the similarities between ours and the labelled “deformed state” are apparent in the increased width at the base, and the elongated trail above shown by the upper part of the image is also mirrored in our initial condition. This reinforces the idea that the model investigated thus far is a realistic interpretation of the spreading action for a droplet like this under specific conditions in the real world.

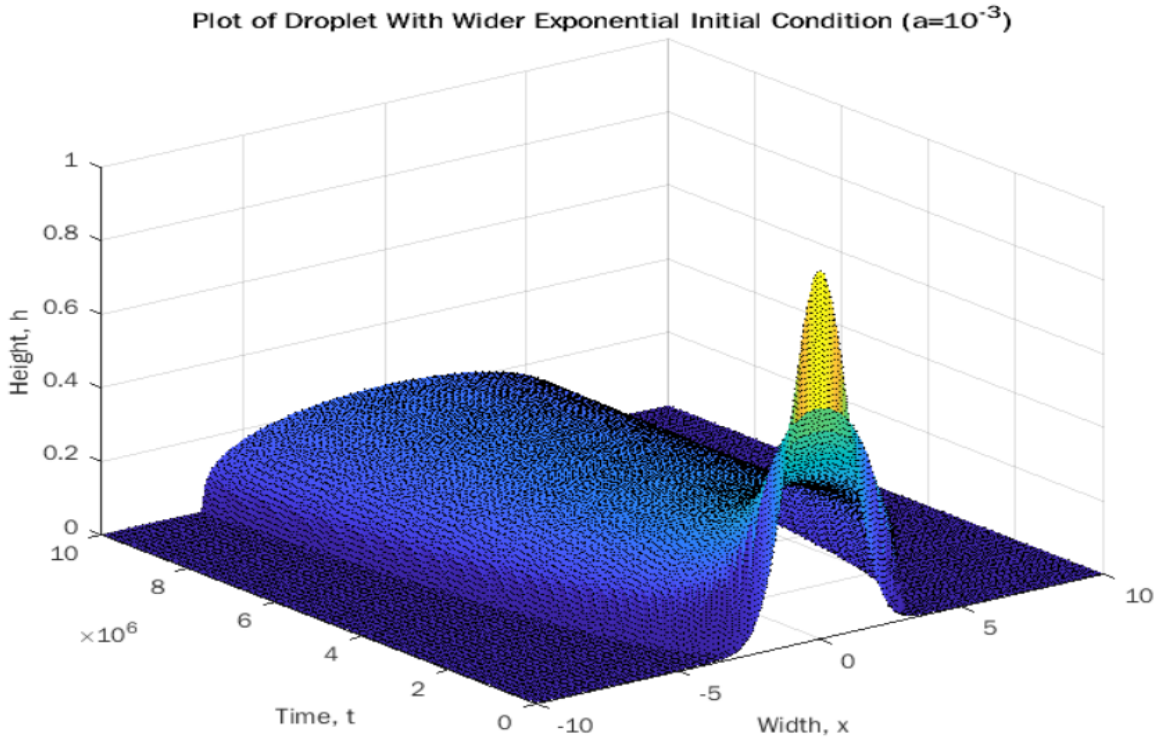
5.1 Initial Width and Alternate Functions

To investigate droplets under different conditions, one can start with increasing the width of the droplet, so we can use $e^{-x^2/2} + 10^{-3}$ instead to increase just the width but retaining the initial drop height, as such

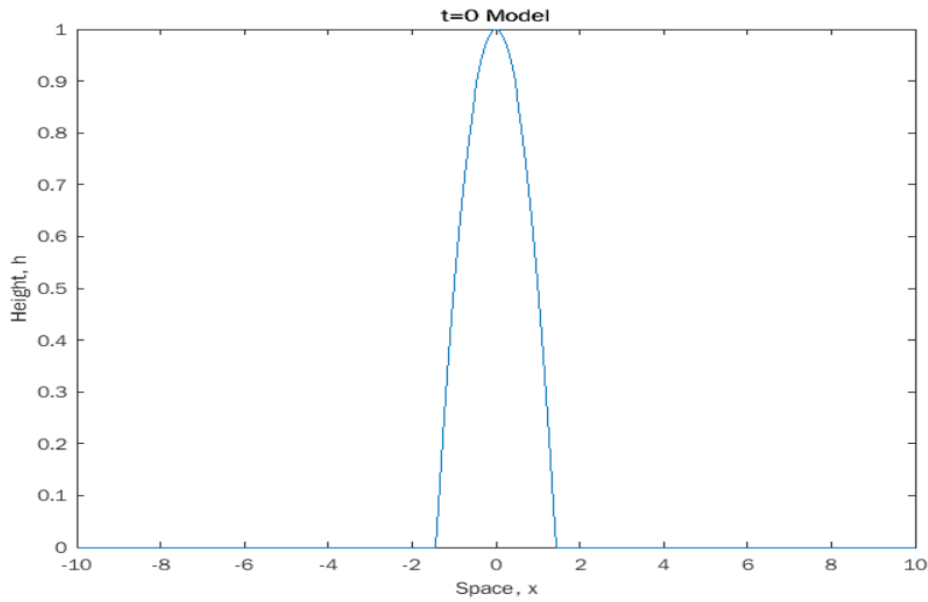


Which, as shown below, increases the rate of spreading since the contact line is wider than

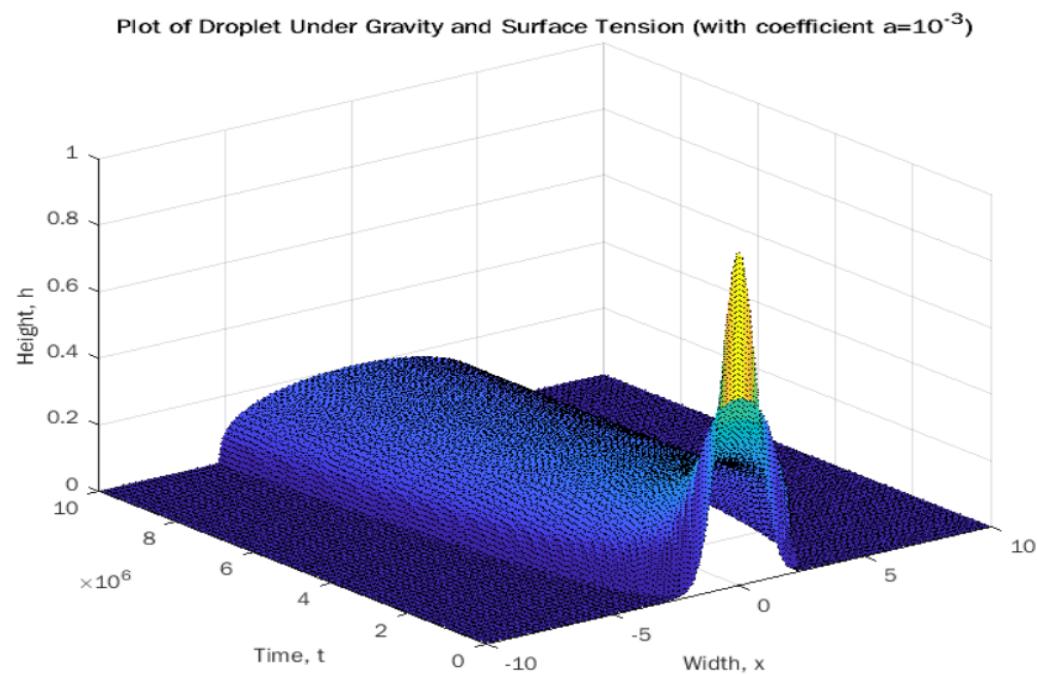
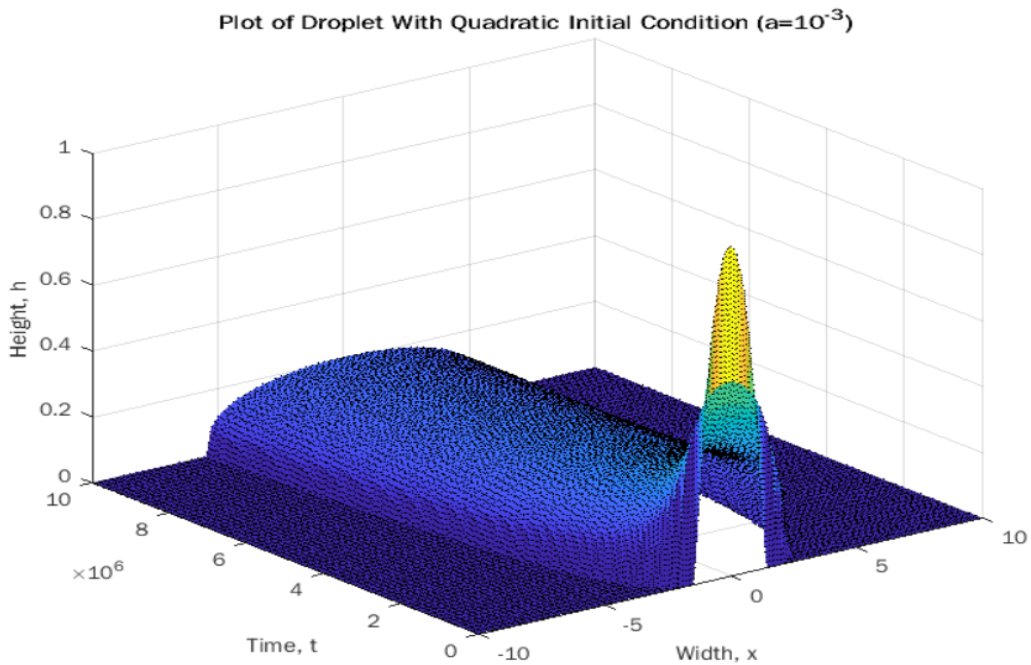
that of the original initial condition.



An alternative to this is by changing the exponential into a quadratic term, e.g. $1 - x^2/2$ for $h = 0$ when $h(x) < 0$, as such



Which removes the run-off at the base, and changes the shape of the outer edge, but has little effect on the overall model, which is evident when placed side-by-side with the original initial condition state

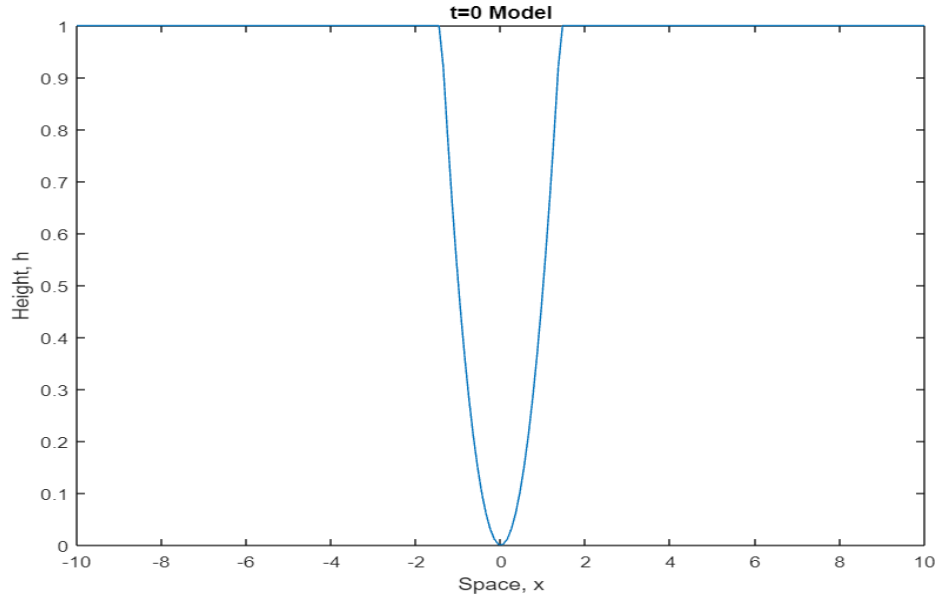


Which shows that both initial states give the same spreading rate, irrespective of the run-off at the base, as long as they start with similar width.

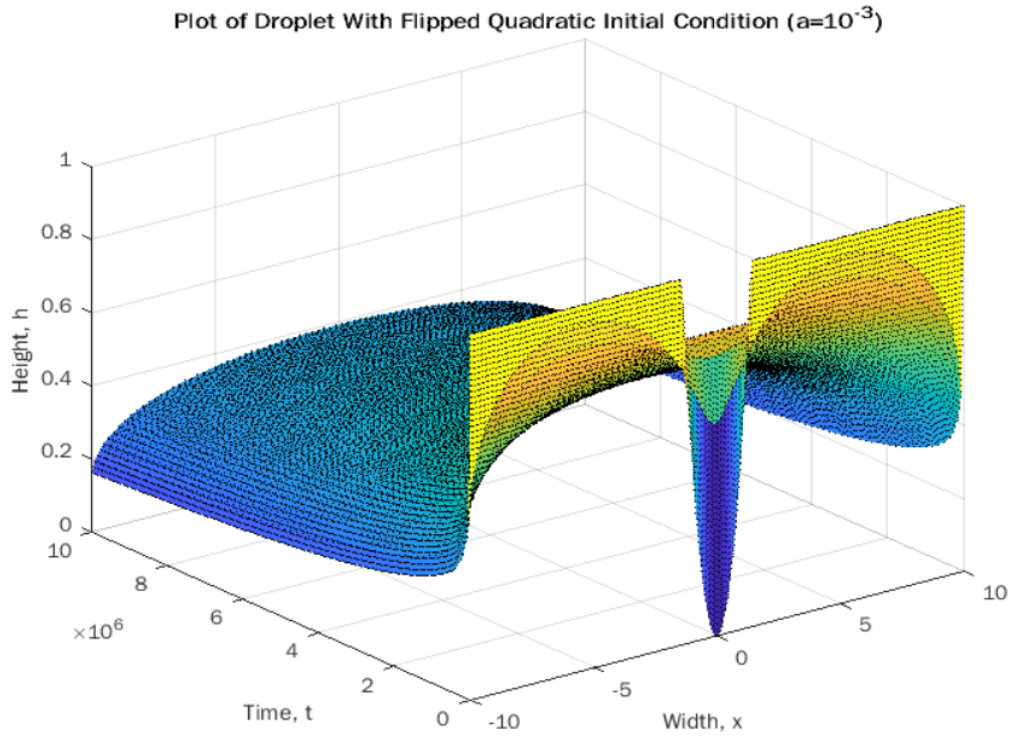
5.2 Setting Initial State Before Contact

So far, only initial conditions that are already at the base have been investigated, which is a symptom of this model. To show why one can't use this model the droplet as it's falling,

which is useful in many contexts, e.g. to simulate rainfall before it makes contact with the ground, one can instead use the reverse of the quadratic model, e.g. $x^2/2$ and $h = 10^{-3}$ for $h(x) > 1$, which looks like



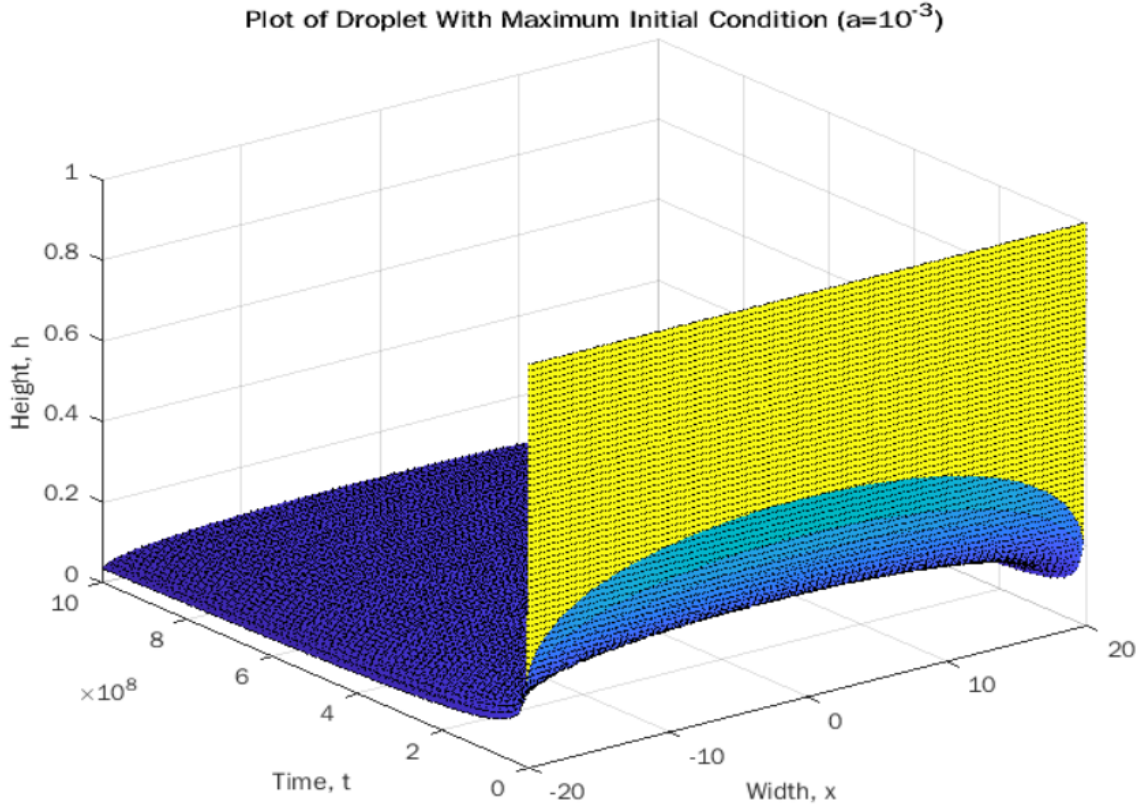
Which looks like a standard droplet shape, except when plugged into the PDE it uses the area underneath the droplet, and hence gives the shape



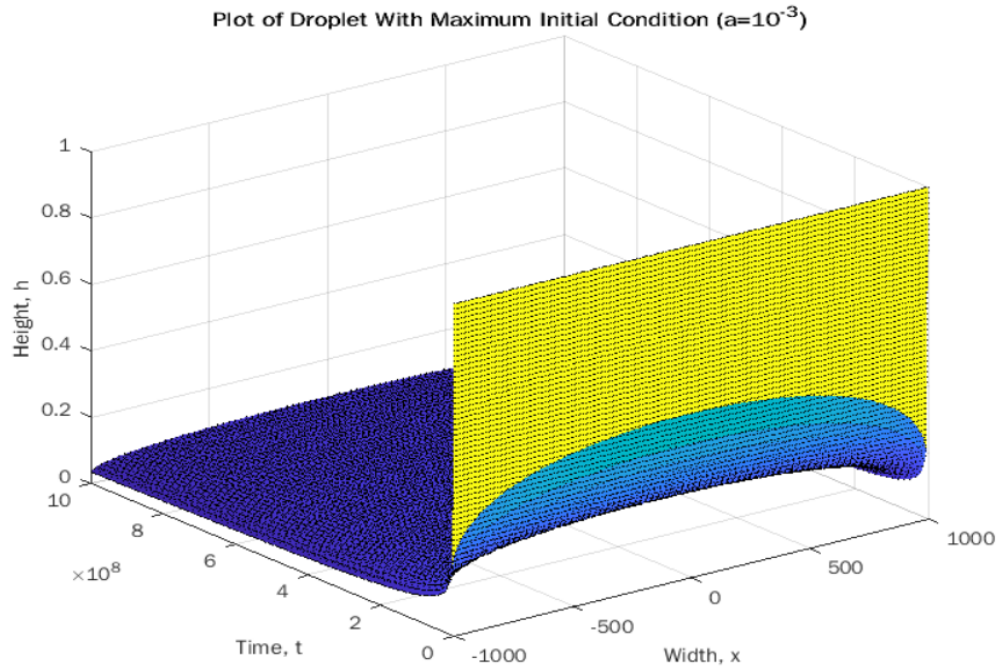
Which shows an impossible droplet pattern, and hence only patterns that are explicitly decreasing functions for $|x|$ are viable.

However, This shows how releasing droplets the same width as the model width gives a false-

looking uniform spreading pattern for the same time frame as the original model, which when plotted instead for just $h = 1$ for $x \in [-20, 20]$, on a larger time scale, one gets:



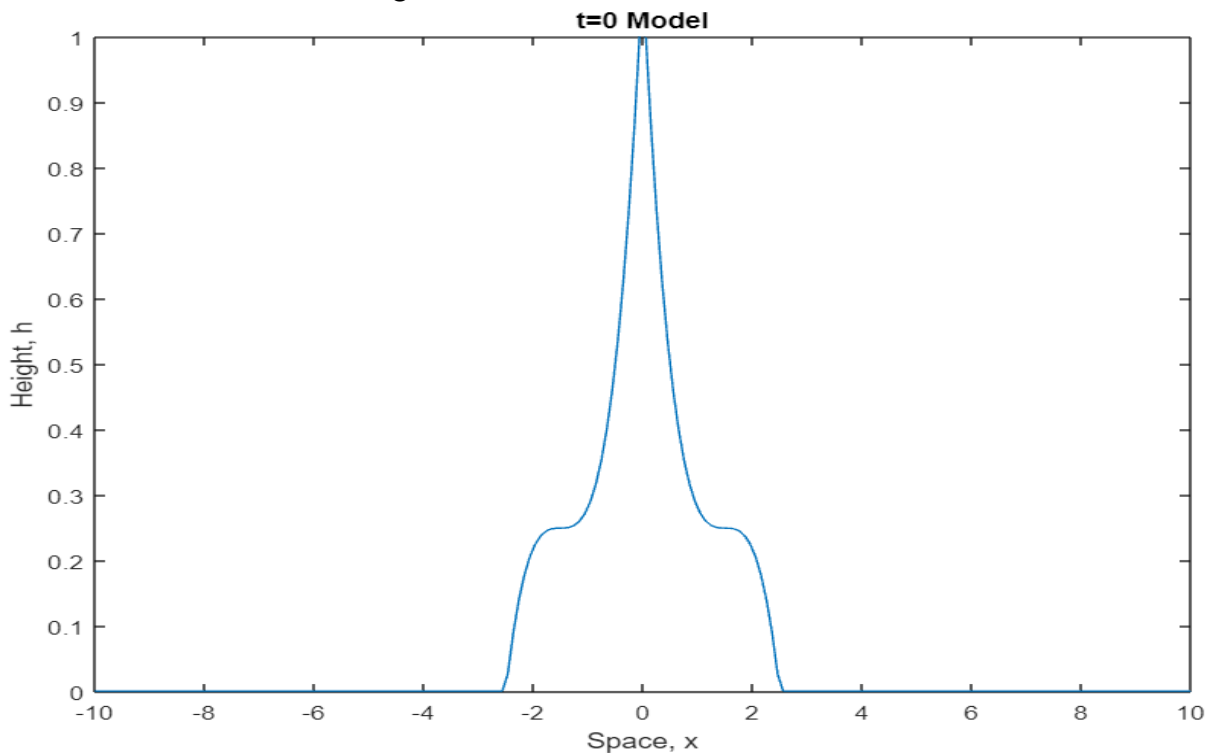
Which shows a much faster initial rate of spreading, with the centre of the drop site decreasing much faster than before, but the entire system still takes much longer to spread the droplet, as is evident in the model looking identical for a much larger width of $x \in [-1000, 1000]$:



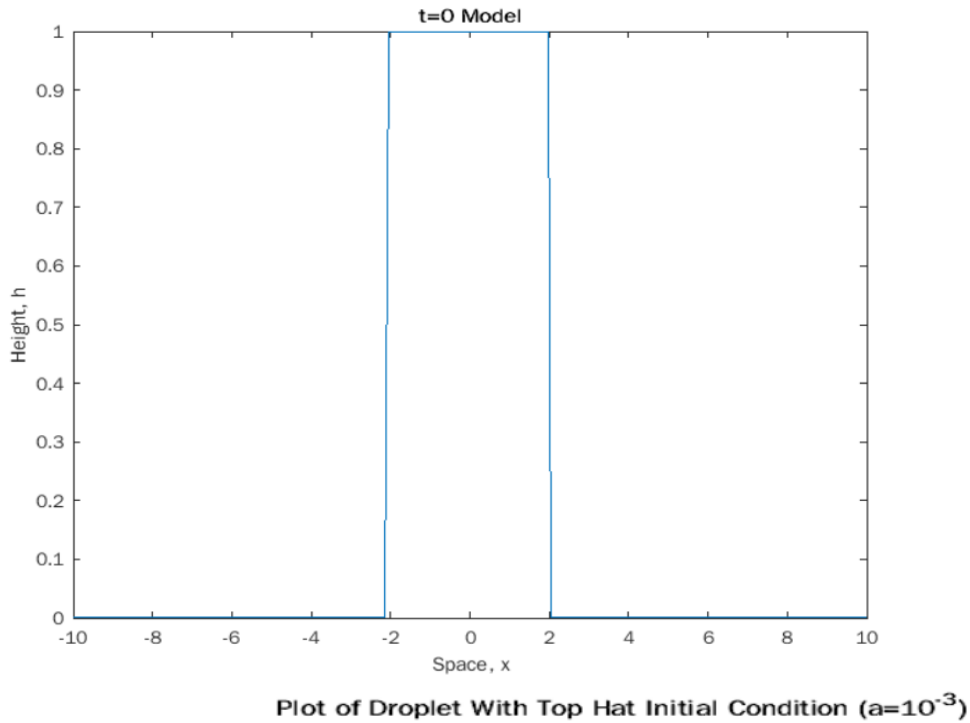
And so contrary to expectation, the amount of water either side of the $x = 0$ line does not slow down the spreading rate in the middle, but instead may even speed it up if this model is a realistic interpretation of the dynamics caused by dropping a large volume of water at once. This is potentially due to tension between water particles, pulling them outward from their initial position.

5.3 Unrealistic Initial States

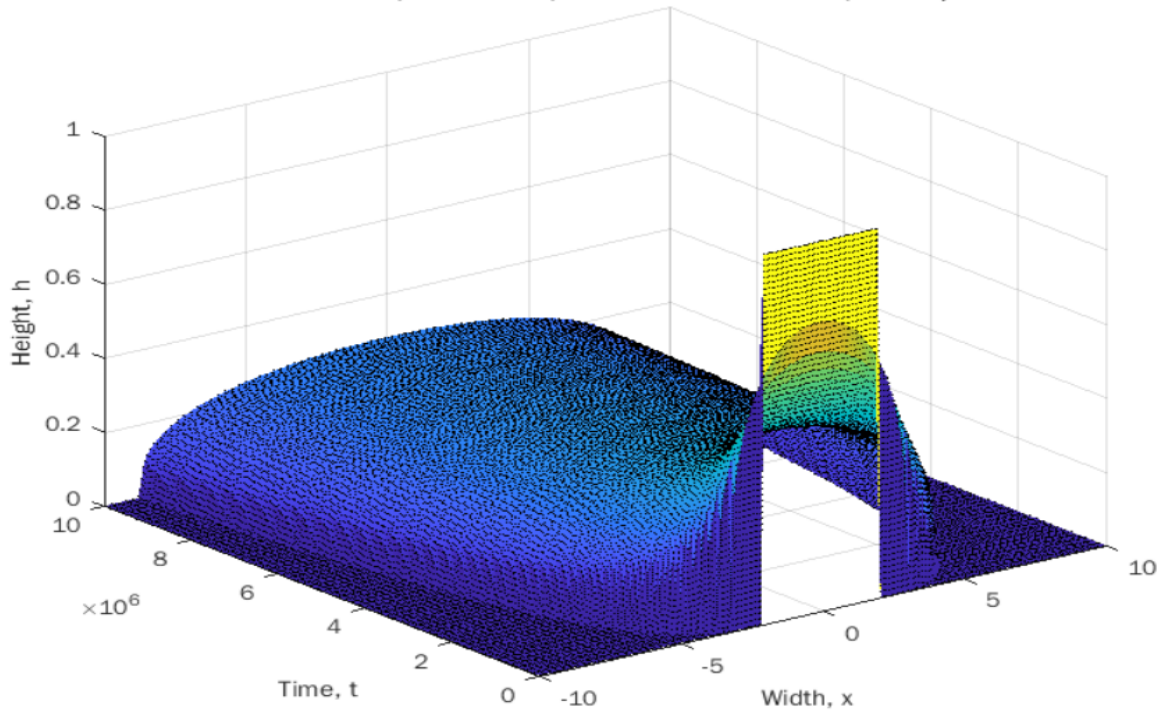
Finally, one can apply a composite function to create a static droplet with extra fluid being added, such as in $\frac{1+(x+\frac{3}{2})^3}{4}$ for $x < 0$, $\frac{1-(x-1)^{\frac{3}{2}}}{4}$ for $x > 0$ and 10^{-3} for everywhere negative under these conditions, which gives



Which is a more bottom-heavy version of the original condition but with a similar overall area, however interestingly the surface plot for this is very similar in spreading rate to the original function. This suggests that the intuitive expectation that the volume of the droplet is the main defining condition on spreading rate may also be supported in this model. To investigate this further, a function with an easily scalable volume must be found. For this task, one can use a two-sided Heaviside function, modelled by $h = 1$ for $x \in [-2, 2]$ and 10^{-3} otherwise, which is unrealistic in context, but will produce standard surface plots that can be analysed.



Plot of Droplet With Top Hat Initial Condition ($a=10^{-3}$)

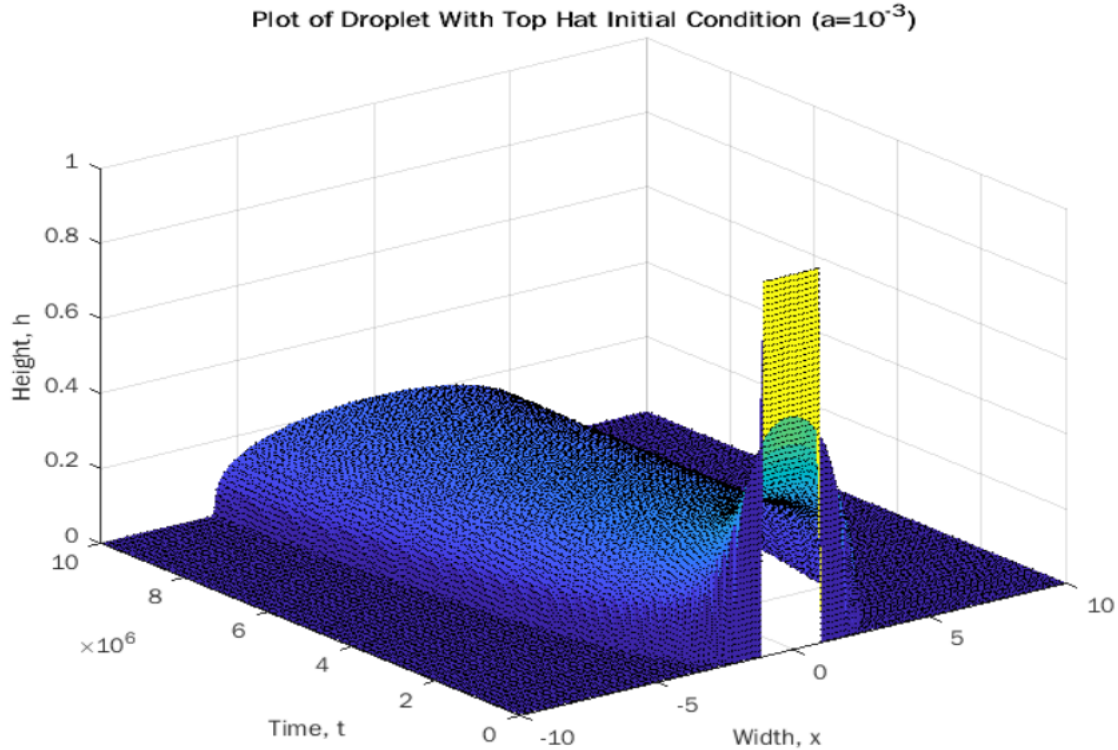


Which obviously spreads faster than the other initial conditions due to the huge mass of the droplet at $t = 0$, but most notably the initial decrease along $x = 0$ is slower than before, which is realistic in context as the volume of water either side is restricting how fast the water at the drop site can spread.

This example is more useful than the realistic situations as changes to the shape of the front have an obvious affect on the total area of the droplet (area as the model is in one-dimensional

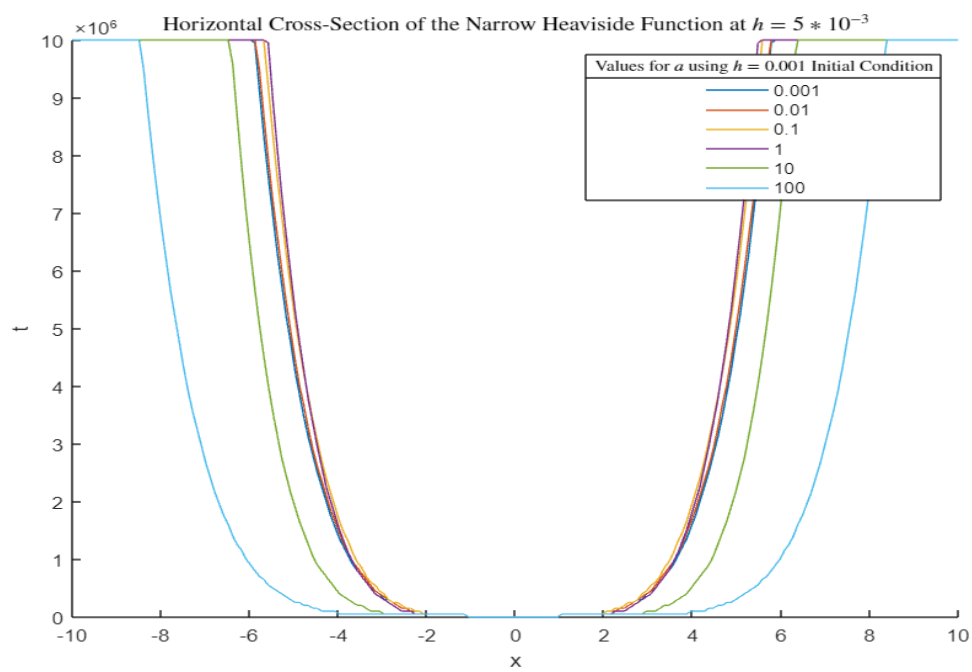
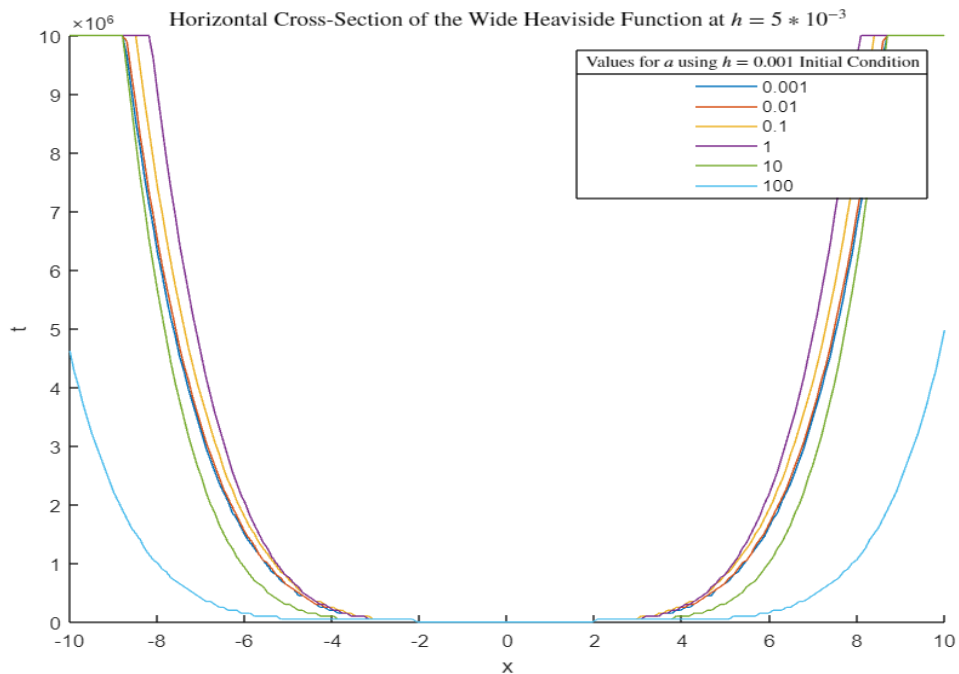
space) so one can investigate changing the width and length to observe the effects on the initial drop-off and of the overall spreading rate.

To make the rate similar to the prior cases, one must decrease the width to $x \in [-1, 1]$ to give



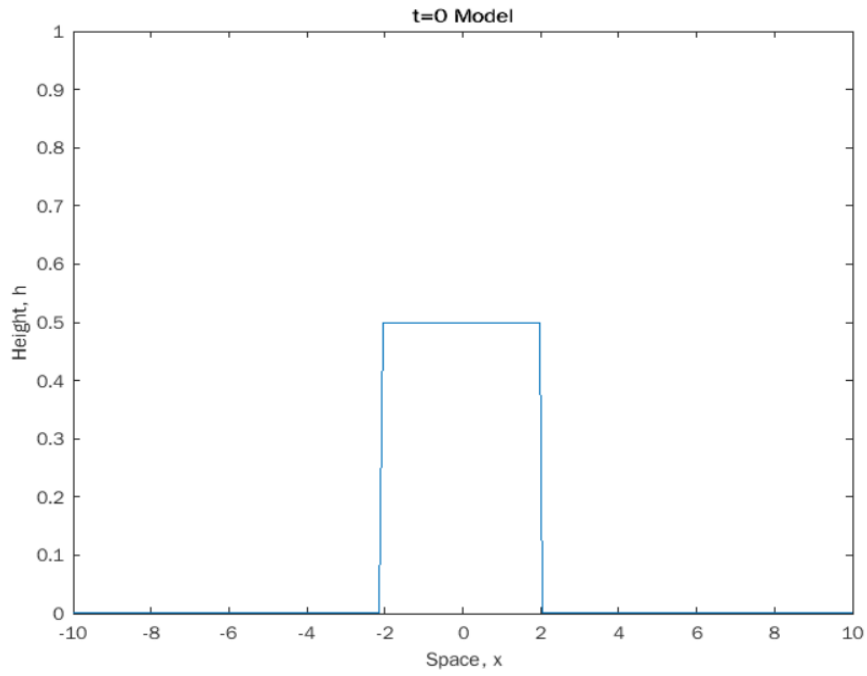
Which takes the same form as the prior plots but for an unrealistic initial case. This shows that halving the width of the droplet here had a dramatic effect on the spreading rate, as it was about half the speed of the previous case.

This is more evident when plotting the corresponding contact-line plots for these functions, as such

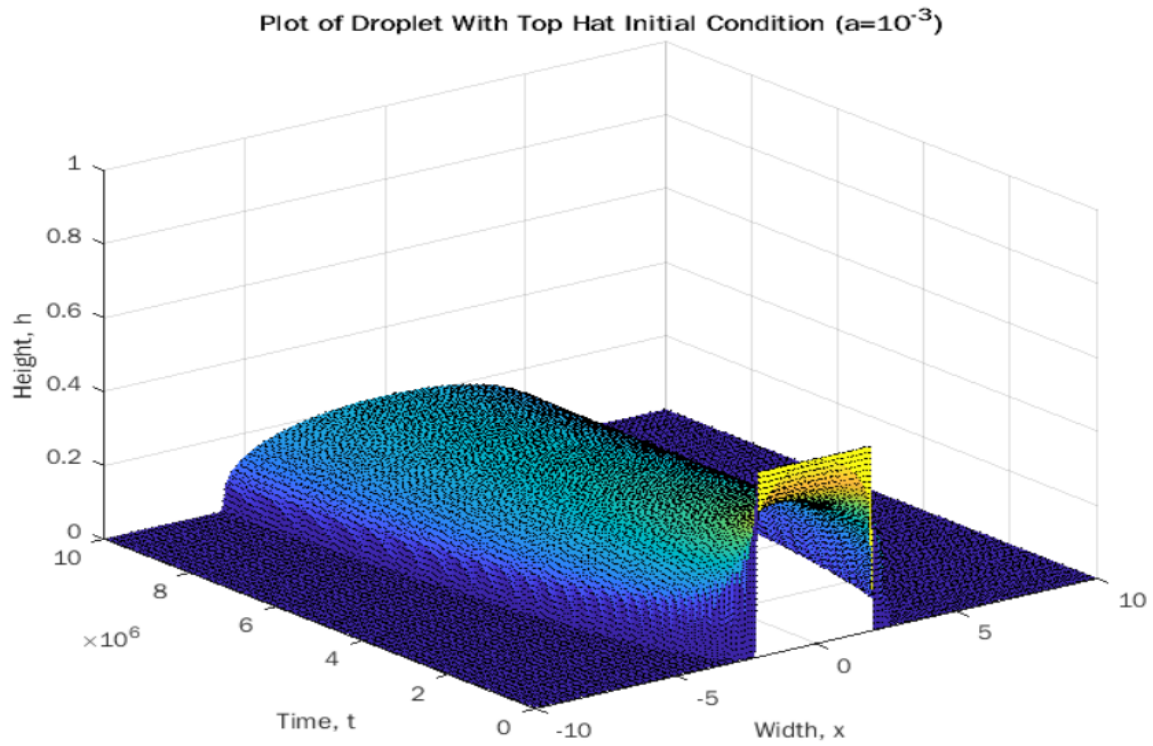


Which shows how for any given proportion of forces (choice of α), the narrow Heaviside function has spread less than the wider case, and that the rate of spreading is increasing due to the slopes of each “quadratic”.

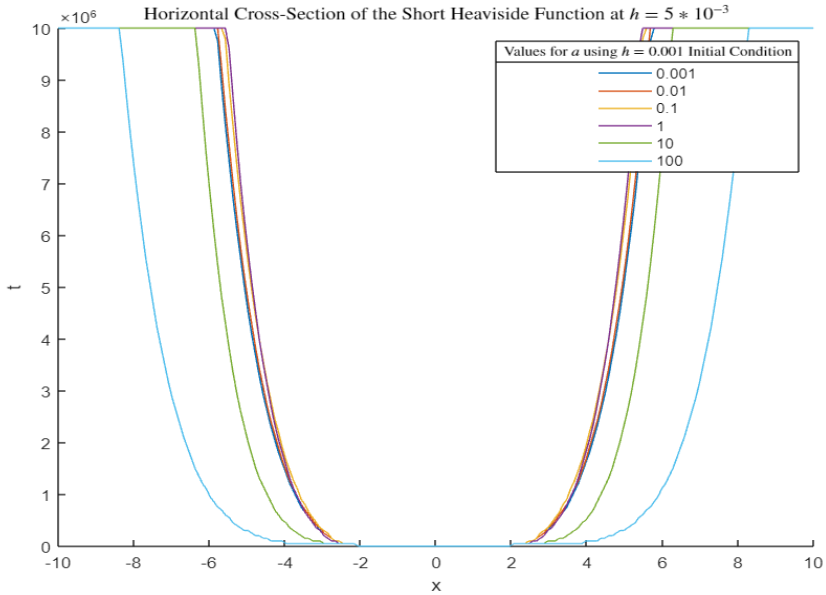
One can also match the original states' rate of decline by using the first x range, but at a lower initial height, e.g. $h = \frac{1}{2}$ in the range and $h = 10^{-3}$ outside, which looks like



Giving a surface plot that looks similar to the realistic situations modelled prior



This shows how decreasing the droplet height, otherwise called the vertical length of the droplet upon release, the rate of spreading decreases. The ratio of decrease is here shown to be



Which is almost identical to the case of halving the width of the Heaviside, except for a marginal increase in spreading rate for the short function relative to the former case, and therefore logically by the area of both the narrow and short functions also being equal, one can assume that the spreading rate of the droplet according to this PDE system under gravity and surface tension (with a given ratio for these forces) is predominantly determined by the initial area of the droplet.

6 Conclusions

In conclusion, the goal of this review was to investigate the effects of varying the ratio of forces and the initial state on the contact-line, the rate of decline at the drop-site, and the spreading rate examined at discrete time intervals.

Overall, it has been shown that varying between gravity and surface tension being the only driving force has little difference, so long as the tensional force is strong enough (around $a = 100$ in section 3.2). However, in this investigation, the forces were used in conjunction, and without a frictional force, to show that the additional tension force under realistic proportions, found to be $a \approx 10^{-3}$ in section 4.2, to gravity has a small effect at the contact-line of the droplet and the surface, and since mass above the surface is conserved, this has a reciprocal effect on the drop-site. Further investigation into the effects of adding a realistic frictional force alongside gravity and tension is required to form a model for different surfaces

and/or different fluid viscosities.

This investigation led into testing the effects of increasing the arbitrarily chosen 10^{-3} boundary condition outside the contact line with the surface, which showed that the model was only suitable for $O(10^{-3})$ and below boundary conditions, and surfaces with greater “wettability”, or more generally hydrophilic surfaces with a contact angle $< 90^\circ$. Therefore further investigation is needed to find a model, or variation of the existing model that accounts for droplets that can reach a resting state with obtuse contact angles.

Next, the action specifically at the centre of the drop-site was examined to see firstly whether changing the ratio of forces had a uniform effect on the spreading rate, and secondly if the decrease was logarithmically linear. Surprisingly, increasing the coefficient of surface tension didn't just increase the rate of spreading at all times (except for $a = O(100)$ and above), and instead showed that varying a around $O(1)$ was the slowest of all orders to decrease, with small increases in a causing an increase in the rate of spreading in height on the small time-scale and a decrease in rate on the large time scale, whereas for orders greater than $O(1)$, the increase still causes a uniform increase in rate of spreading initially but plateaus to the same rate as the latter $O(1)$ terms for all further times, and vice versa for lower orders of a . Logarithmically speaking, the exact solution investigated in section 2.1 showed that the gradient for large t should be linear and consistent, which is shown to be true here for all realistic force ratios prior to $a = O(1)$ beyond each of their respective threshold time values. This is supported by further investigation into cross-sections at spatial values other than the drop-site, where even points that were not within the initial condition domain underwent the same shift around this a value, which overall suggests that at this order, the surface tension force starts to become the dominant force in the system.

This constant logarithmic gradient is also true for the contact line plots, meaning any increase in a must have a logarithmically increasing effect on the shape of the contact line, and hence on the rate of fluid dispersion, which is supported by the finding that increasing a has diminishing returns on the rate of increase of the spreading, due to geometric increases in a on the logarithmic contact-line giving approximately the same linear translation in time on this scale. The last variable thus far unchanged has been the initial state, which has used an exponential

function to model the droplet at some point after it makes contact with the surface. It is shown that the model is insufficient for times prior to this, as the initial condition must have a decreasing height as x increases in either direction, since the PDE treats the droplet as the area under a defined line; and since there are no frictional forces examined in this model, so this would make the model too abstract. This leaves room for further investigation into a PDE model that can handle water droplets before and after contact with the surface.

However, further investigation into the system after having made contact suggested that changing the size of the droplet would have a profound effect on the spreading rate, so the original exponential model was changed to a less realistic Heaviside function so that the effects of changing the height, width and overall area became more pronounced. With these changes, it is shown that halving the width and halving the height have almost the exact same effect on the spreading rate, and so it became logical to assume that the spreading rate is directly related to the mass (initial area) dropped.

Overall, despite assuming no friction or absorption, and using a relatively low resolution approximation, this model has shown that it acts similarly to expectations for a hydrophilic, non-porous surface in regard to the rate of fluid dispersion when taking small boundary conditions of order 10^{-3} with a smaller ratio of tension to gravity.

A Raw data

A.1

A table of the percentage error between the true value of the heat equation, and the method of lines approximation at specific times and positions for just 200 steps (a relatively low resolution):

$\downarrow Time/Space \rightarrow$	0.25	0.3	0.35	0.4	0.45	0.5	0.55	0.6	0.65	0.7	0.75
0.05	0.72	0.4	0.19	0.06	0.01	0.03	0.01	0.05	0.18	0.37	0.68
0.1	1.25	0.92	0.7	0.56	0.48	0.45	0.47	0.54	0.68	0.89	1.21
0.15	1.81	1.48	1.27	1.13	1.05	1.02	1.04	1.12	1.25	1.46	1.77
0.2	2.39	2.06	1.84	1.7	1.62	1.59	1.62	1.69	1.82	2.03	2.35
0.25	2.92	2.59	2.38	2.24	2.16	2.13	2.16	2.23	2.36	2.57	2.88
0.3	3.46	3.14	2.92	2.79	2.71	2.68	2.7	2.78	2.91	3.11	3.42
0.35	4.0	3.68	3.47	3.33	3.25	3.23	3.25	3.32	3.45	3.65	3.96
0.4	4.47	4.15	3.94	3.8	3.72	3.7	3.72	3.79	3.92	4.12	4.43

A.2

A table of different hydrophobic components and their respective contact lines using different methods of measurement [4]:

Hydrophobic component	Short form	Contact angle β ($^{\circ}$)	
		Photography method	Counting method
Methyltrimethoxysilane	MTMS	95	94
Dimethylchlorosilane	DMCS	98	100
Dimethyldichlorosilane	DMDC	120	119
Trimethylchlorosilane	TMCS	—	—
Trimethylsilylchloroacetate	TMSCA	—	—
Trimethylbromosilane	TMBS	—	—
Trimethylmethoxysilane	TMMS	125	123
Trimetyletoxysilane	TMES	102	100
Tetramethylsilane	TMS	0	0
Hexamethyldisilane	HMDS	135	133

References

- [1] Xoviabcs YouTube, <https://www.youtube.com/watch?v=FqKLoO19kwo>, Accessed 20/10/21.
- [2] Mathworks, Matlab Documentation: 'pdepe', 'ode15s' and 'ode45',
<https://uk.mathworks.com/help/matlab/ref/pdepe.html>,
<https://uk.mathworks.com/help/matlab/ref/ode15s.html>,
<https://uk.mathworks.com/help/matlab/ref/ode45.html>, Version 2021b
- [3] Aerogel Homepage, <http://www.aerogel.org/>, Accessed 24/11/21
- [4] Kupiec, Katarzyna; Konieczka, Piotr and Namienik, Jacek (2009), 'Characteristics, Chemical Modification Processes as well as the Application of Silica and its Modified Forms', Critical Reviews in Analytical Chemistry, 39:2,60 — 69, Accessed 25/11/21
- [5] Singh, Gaurav, 'The Optical Trek Through a Scientific Lens',
<https://myopticaltrek.wordpress.com>, Accessed 25/12/21
- [6] Joshi, Sumit, 'The Shape of a Water Droplet', <https://towardsdatascience.com/the-shape-of-a-water-droplet-cb902b69e9cb>, Accessed 25/12/21
- [7] Wikipedia, 'Wetting', <https://en.wikipedia.org/wiki/Wetting>, Accessed 28/12/21
- [8] Montajar Sarkar, Muhammad Hasanuzzaman, Fahmida Gulshan, Arhm Rashid, Surface, Mechanical and Shape Memory Properties of Biodegradable Polymers and Their Applications, Reference Module in Materials Science and Materials Engineering, Elsevier, 2020, ISBN 9780128035818, <https://doi.org/10.1016/B978-0-12-820352-1.00050-X>. (<https://www.sciencedirect.com/science/article/pii/B978012820352100050X>) Accessed 28/12/21
- [9] Gundersen, Håkon; Leinaas, Hans; Thaulow, Christian. (2014). 'Surface Structure and Wetting Characteristics of Collembola Cuticles'. PloS one. 9. e86783. 10.1371/journal.pone.0086783. <https://www.researchgate.net/figure/Contact-Angles-The-contact->

angle-is-defined-as-the-angle-between-the-droplet-and-the_fig11_260108973. Accessed 28/12/21

[10] Lizhuang Chen, Xueying Li, Chapter 4 - Sodium battery nanomaterials, Editor(s): Fen Ran, Shaowei Chen, In Micro and Nano Technologies, Advanced Nanomaterials for Electrochemical-Based Energy Conversion and Storage, Elsevier, 2020, Pages 115-160, ISBN 9780128145586, <https://doi.org/10.1016/B978-0-12-814558-6.00004-6>.

(<https://www.sciencedirect.com/science/article/pii/B9780128145586000046>) Accessed 28/12/21

[11] Carlos M. Costa, Yong-Hyeok Lee, Jung-Hwan Kim, Sang-Young Lee, Senentxu Lanceros-Méndez, Recent advances on separator membranes for lithium-ion battery applications: From porous membranes to solid electrolytes, Energy Storage Materials, Volume 22, 2019, Pages 346-375, ISSN 2405-8297, <https://doi.org/10.1016/j.ensm.2019.07.024>.

(<https://www.sciencedirect.com/science/article/pii/S2405829719308840>) Accessed 28/12/21